8-2024

Impact of Nitrogen Species on Algal Carbon Capture

Lauren J. Todd
Clemson University, ljtodd@clemson.edu

IMPACT OF NITROGEN SPECIES ON ALGAL CARBON CAPTURE

A Thesis
Presented to
the Graduate School of
Clemson University

In Partial Fulfillment
of the Requirements for the Degree
Master of Science
Biosystems Engineering

---

by
Lauren Juliana Todd
August 2024

Accepted by:
Dr. Caye Drapcho, Chair
Dr. Mary Katherine Watson, Co-chair
Dr. Yu-Bo Wang
Dr. Tom Owino

ABSTRACT

Increasing global carbon emissions from fossil fuel combustion and the resulting detrimental effects of climate change have created a need for atmospheric carbon drawdown. Biological-based carbon capture not only sequesters carbon dioxide (CO_2) but also provides a sustainable source of biomass for biofuels and biomaterials. Thus, the aim of this research was to examine freshwater green algal growth with total ammoniacal nitrogen (TAN) and nitrate nitrogen (NO_3-N) sources at high pH for improving carbon capture potential. The following objectives were accomplished: nitrogen uptake was identified as simultaneous or sequential, the effect of TAN and NO_3-N on culture pH was quantified, and kinetic and stoichiometric growth parameters were examined for the two nitrogen sources.

The literature review discusses the impact of TAN and NO_3-N on algal growth and culture pH, in which autotrophic algal growth using TAN lowers culture pH by producing H^+ ions, and NO_3-N raises pH by consuming H^+. The Monod model kinetic constants from microalgal growth studies are summarized for each nitrogen source, and inhibitory levels of TAN are compiled. The properties of carbonate equilibrium reactions with passive CO_2 diffusion, enhanced CO_2 diffusion in alkaline systems, and subsequent inorganic carbon-limited algal growth are presented to justify a high culture pH design.

Scenedesmus sp. growth was observed in open reactors with various TAN and NO_3-N treatment ratios. Specific growth rates were analyzed based on three identified phases of growth based on nitrogen and carbon substrate utilization. The highest specific growth rates were observed during phase one with TAN utilization and peak observed

carbon, with an average of 0.043 hr^{-1} that was not impacted by initial TAN. Biomass yields on a nitrogen basis were assessed based on periods of TAN or NO_3-N use. In reactors containing both nitrogen sources, TAN was utilized preferentially by the algae with NO_3-N utilization after TAN depletion. The culture pH was stable during TAN consumption and rose once NO_3-N was used; the peak pH for the largest TAN:NO_3-N ratio was 10.990, while the peak pH for the NO_3-N only treatment was 11.319. The results of this study can aid the design of algal cultivation systems for carbon capture, specifically the application of NO_3-N and TAN as a biological pH control method to optimize both carbon capture and algal growth.

DEDICATION

This thesis is dedicated to my parents, David and Jackie, and my sister, Miranda, whose endless support has been the foundation for all my pursuits in life.

ACKNOWLEDGMENTS

I would like to give my deepest gratitude to my advisors, Drs. Mary Katherine Watson and Caye Drapcho, for their mentorship and encouragement. Their fundamental research with algal carbon capture has allowed for the advancement of this study. It has been an honor to learn from them, which I anticipate continuing in the future. Additionally, thank you to my committee members, Drs. Yu-Bo Wang and Tom Owino, for your assistance with this research and my education.

For chemical instrumentation aid and maintenance, I thank Dr. Daekyun Kim at Rich Laboratory. I thank Dr. Shannon Alford and other research associates at Clemson University Agriculture Service Laboratory for their sample analysis. For allowing the use of their ion chromatography column and instrumentation assistance, I thank Dr. David Ladner and Carl Espinosa. Lastly, I thank the Department of Environmental Engineering and Earth Sciences, and the National Science Foundation for financial support.

TABLE OF CONTENTS

Page

LIST OF TABLES

LIST OF FIGURES

CHAPTER ONE

INTRODUCTION

Introduction

In 2023, a new record for global carbon dioxide (CO_2) emissions was set at 37.4 billion tonnes, with 65% of the increase due to coal emissions (IEA, 2024). In addition to researching novel ways to reduce our dependence on fossil fuels and advocating for green technologies, the level of CO_2 currently emitted to the atmosphere must be addressed to reduce the severity of global warming due to the greenhouse gas. Direct carbon capture technologies, including physical or chemical absorption of CO_2 from point source pollution, can be energy intensive, expensive, and require a storage method for captured carbon (Farrelly et al., 2013). Biologically based carbon capture is unique in that separation and storage of CO_2 occur within the same mechanism of biomass growth, which can then be utilized as sustainable biofuels or biomaterials to replace fossil fuel-dependent products. Where biomass from land-based vegetation has been criticized for occupying arable land needed for food sources and depending on a growing season, microalgae biomass requires neither (Dalrymple et al., 2013; Kumar & Bera, 2020). However, microalgal cultivation does require water, nutrients, and energy for biomass harvesting. Some research has focused on wastewater streams to provide water and nutrients such as nitrogen and phosphorous, which can also aid with pollutant removal requirements for wastewater (Dalrymple et al., 2013). Especially in municipal wastewater with both total ammoniacal nitrogen (TAN) and nitrate nitrogen (NO_3-N) present, the

preferred nitrogen source for algal growth must be established for successful modeling and design.

Microalgae can use both TAN and NO_3-N sources, with autotrophic growth using TAN lowering culture pH by producing H^+ ions and NO_3-N raising pH by consuming H^+ (Dalrymple et al., 2013; Markou et al., 2013). Uptake of either nitrogen source, when both are available, can also be classified as simultaneous or sequential. Algal utilization of TAN, being the sum of ammonium nitrogen (NH_4-N) and ammonia nitrogen (NH_3-N), is less energy-demanding for anabolic metabolism but is toxic to algal growth (Collos & Harrison, 2014; Sanz-Luque et al., 2015). NH_3 is the most toxic of the two TAN species, so a distinction is made between the two for discussion of toxicity and impact on growth.

The removal of CO_2 from the atmosphere for microalgal carbon capture is achieved through passive diffusion into the growth medium, which can be enhanced by an alkaline culture pH (Watson & Drapcho, 2016). Using the physiological process of algal TAN and NO_3-N growth, a method of pH control can be implemented to maintain enhanced CO_2 diffusion kinetics. At high pH, most of the inorganic carbon is present as bicarbonate (HCO_3^-) or carbonate (CO_3^{2-}); thus, *Scenedesmus* sp., a freshwater green microalgae species, was chosen for this study due to its ability to utilize multiple inorganic carbon substrates, high lipid content for potential high-value bioproducts, and tolerance to high pH (Watson & Drapcho, 2016; Maryshamya et al., 2019).

Therefore, investigation of microalgal-based carbon capture with various nitrogen sources at high pH is necessary to design and apply large-scale, efficient systems to draw down carbon. The following objectives of this research will be accomplished:

i. Identify nitrogen uptake preference as simultaneous or sequential in cultures with mixed nitrogen sources.

ii. Quantify the effect of NO_3-N and TAN as single and mixed nitrogen sources on culture pH.

iii. Quantify the effect of NO_3-N and TAN as single and mixed nitrogen sources on kinetic and stoichiometric growth parameters.

Literature Review

Impact of Nitrogen Species

For nitrogen assimilation, NO_3-N and TAN can both be utilized in microalgae; thus, they are classified as substitutable substrates (Drapcho et al., 2020; Markou et al., 2013; Lachmann et al., 2019). However, the preferred nitrogen source for optimal growth depends on numerous factors such as algal species, pH, growth conditions, and other nutrient and substrate availability (Lachmann et al., 2019). Theoretically, TAN utilization would be more metabolically advantageous than NO_3-N as the nitrogen in TAN molecules is at the oxidation state (-III) required for amino acid synthesis (Collos & Harrison, 2014; Sanz-Luque et al., 2015). Transport enzymes regulate NO_3-N intake into algal cells and requires two reduction steps: first a nitrate reductase (NR) enzyme uses ATP to convert nitrate to nitrite in the cytoplasm, followed by conversion of nitrite to ammonium via a nitrite reductase enzyme in the chloroplast (Sanz-Luque et al., 2015). Thus, with no reduction required for TAN assimilation, it is less energy intensive and

would be preferentially utilized by algae. Some studies have found substrate availability is a better indicator for nitrogen source utilization, specifically carbon and phosphorous molecules necessary for cellular energy production (Lachmann et al., 2019). Lachmann et al. (2019) found that the difference in photosynthetic efficiency for NH_4^+ and NO_3^- was reduced in replete carbon and phosphorous conditions, with NO_3^- efficiency being only 6% greater than NH_4^+.

In environments where TAN and NO_3-N are present, algal consumption can be further distinguished as simultaneous or sequential. The NR enzyme and its genetic expression are generally repressed in the presence of TAN and induced with NO_3-N (Sanz-Luque et al., 2015; Kumar & Bera, 2020). Though studies have observed sequential use with TAN consumed first (Kumar & Bera, 2020), the enzymatic function is not binary. Instead, it is more probable that TAN is less repressive with high levels of NO_3-N, on the magnitude of mM concentrations (Sanz-Luque et al., 2015). The TAN threshold that results in total NR suppression is species-specific, but for natural oyster-pond populations, a concentration higher than approximately 0.0021 mM NH_4-N prevented NO_3-N uptake (Maestrini et al., 1986). The same study also observed that the rate of NO_3-N uptake reached a maximum when NH_4-N concentration was below 0.00054 mM, indicating that simultaneous utilization is possible at low enough TAN concentrations (Maestrini et al., 1986).

A major effect of the nitrogen source on algal growth and carbon capture potential is the impact on the culture pH. Autotrophic algae grown with NO_3-N consume H^+ and

raise the system's pH, while algae that utilize TAN produce H^+ and lower the pH (Dalrymple et al., 2013; Markou et al., 2013). This biological mechanism can be exploited as a method of pH control in algal cultivation systems, where excessively alkaline conditions, greater than 11.5 pH (Watson & Drapcho, 2016; Watson et al., 2024), created during algal NO_3-N consumption can hinder growth. Subsequently, NO_3-N addition can raise culture pH for enhanced CO_2 diffusion kinetics (Watson & Drapcho, 2016).

Culture pH can also be influenced by interactions between aqueous CO_2 and NH_3, where carbamic acid is rapidly formed and subsequently deprotonates to produce ammonium carbamate at a pH greater than the pK_a of 6.76 (Wang et al., 2011). These reversible reactions are typically associated with a decrease in pH, resulting in carbamate breaking down into ammonium and bicarbonate (Wang et al., 2011). According to Wang et al. (2011), at an initial pH of 10.4, NH_3 can further enhance the conversion of CO_2 to carbonate species, with higher concentrations of NH_3 promoting CO_2 absorption (Qin et al., 2010; Wang et al., 2011). However, challenges can arise as greater NH_3 concentrations result in higher volatility and algal toxicity.

Both forms of TAN, gaseous NH_3 and cationic NH_4^+, are toxic to algal growth, but NH_3 is regarded as the more toxic form since it can passively diffuse into cells, being uncharged and lipid-soluble (Markou et al., 2013; Collos & Harrison, 2014). Due to the charge of NH_4^+, transport into the cell is regulated with enzymes (Collos & Harrison, 2014). The pH significantly influences TAN equilibrium, with more NH_3 present at pH

values greater than the pK_a of 9.25 (Markou et al., 2013). The biological mechanism of NH_3 toxicity is amine uncoupling in chloroplasts and intracellular pH disruption, which completely prevents growth at high concentrations (Crofts, 1966; Wang et al., 2011). One study found that concentrations greater than 3 mM NH_3-N completely inhibited Scenedesmus *obliquus* growth (Abeliovich & Azov, 1976). Table 1.1 lists inhibition levels for various algal species with specifications for the form of TAN investigated, which informed the selection of experimental treatments.

Table 1.1: Summary of TAN toxicity in microalgal growth studies

Authors	**Algal Species**	**pH**	**Inhibitory Level (mM)**	**TAN Species Reported**
Abeliovich & Azov (1976)	*Scenedesmus obliquus*	8	2	NH_3-N
Azov & Goldman (1982)	*Scenedesmus obliquus*	8-9.5	1.2	NH_3-N
Bohutskyi et al. (2016)	*Scenedesmus actus f. alternans* and *Scenedesmus dimorphus*	6.9-7.2	11.4	NH_3-N
Collos & Harrison (2014)	*Chlorophyceae*	N/A[1]	7.6	NH_4-N
Ip et al. (1982)	*Scenedesmus* and *Chlorella*	6.1-9.1	2.9	NH_3-N
Lu et al. (2018)	*Chlorella* sp.	6.0	28.03	NH_3-N
Morales-Amaral et al. (2015)	*Scenedesmus* sp.	8	13.7	NH_4-N
Park et al. (2010)	*Scenedesmus* sp.	8.5	7.13	NH_4-N

[1]Mean inhibition level calculated based on several studies

The modeling of an algal growth system with TAN utilization becomes more complex, with additional interactions between CO_2 and NH_3 as well as NH_3 volatility.

TAN species can be determined for modeling volatilization by measuring pH in the absence of background acids and bases in the chemical matrix, since the correlation between NH_3 loss and pH is independent of volatilization kinetics (Moeller & Vlek, 1982). However, this does not apply to algal growth medias that typically have a complex chemical background. Additionally, Moeller and Vlek (1982) explicitly exclude CO_2 interactions in their stagnant film models since additional reaction rates and kinetic constants would be required for carbamate/carbamic acid formation and dissociation. Supplementary to enhanced CO_2 diffusion kinetics at high pH, mass transfer is also enhanced via chemical absorption with NH_3, a process typically used for direct chemical carbon capture technologies (Qin et al., 2010; Farrelly et al., 2013)

Monod kinetic constants are listed in Tables 1.2 and 1.3 for TAN and NO_3-N utilization, respectively, with various algal species. Often, studies reported substrate uptake kinetics instead of algal growth kinetics, which were not included in the tables. The growth kinetic constants are notably variable depending on species and experimental conditions, though in general, NO_3-N utilization maximum specific growth rates (μ_{max}) were greater than TAN utilization. The half-saturation constants (K_S) were also greater for TAN utilization, indicating a lower affinity for TAN.

Table 1.2: Summary of Monod kinetic constants from microalgal growth studies with TAN

Authors	Algal Species	TAN Treatments (mM)	μ_{max} (1/h)	K_S (mM)
Aslan & Kapdan (2006)	*Chlorella vulgaris*	0.94-29.26	-	2.25
Baldia et al. (1991)	*Spirulina platensis*	0-3.57	0.028	0.018
Eze et al. (2018)	*Desmondesmus* sp.	3.16-11.96	0.0071	-
Gutierrez et al. (2016)	*Neochloris oleoabundance*	0.19-19.69	-	0.19
	Dunaliella tertiolecta	0.19-19.69	-	0.043
Sousa et al. (2021)	Chlorella vulgaris	1.18	0.12	-

Table 1.3: Summary of Monod kinetic constants from microalgal growth studies with NO_3-N

Authors	Algal Species	NO_3-N Treatments (mM)	μ_{max} (1/h)	K_S (mM)
Baldia et al. (1991)	*Spirulina platensis*	0-3.57	0.02	0.086
Eze et al. (2018)	*Desmondesmus* sp.	3.16-11.96	0.0042	-
Padil et al. (2023)	Information not available	11.77-17.65	0.033	0.019
Ribita (2011)	*Scenedesmus dimiorphus*	0.35-3.53	0.029	0.059
Sousa et al. (2021)	*Chlorella vulgaris*	2.25	0.111	-
Xin et al. (2010)	*Scenedesmus* sp.	0.18-1.78	-	0.84

Inorganic Carbon – Limited Algal Growth

Autotrophic algae need inorganic carbon for growth, which is supplied by passive atmospheric CO_2 diffusion into an aqueous medium for carbon capture systems. The simplified reversible reaction of CO_2 diffusion to the dissociation of carbonate in aqueous systems is shown in Equation 1.1 (Stumm & Morgan, 1981). There are four main reaction mechanisms: CO_2 hydration and hydroxylation, and HCO_3^- protolysis and hydrolysis.

$$H_2O + CO_{2\,(g)} \leftrightarrow H_2O + CO_{2\,(aq)} \leftrightarrow H_2CO_3 \leftrightarrow HCO_3^- + H^+ \leftrightarrow CO_3^{2-} + 2H^+ \text{ (Equation 1.1)}$$

The hydration pathways for CO_2 are summarized in Figure 1.1 (Watson et al., 2024). HCO_3^- can be directly formed through path I, or through an intermediate step of path II, forming H_2CO_3, and then the final path III to form HCO_3^- (Eigen et al., 1961; Eigen, 1964). It is impossible to discern which pathway is occurring, however, the equilibrium for path II exists with the majority of aqueous CO_2 unreacted, so H_2CO_3 is either ignored or combined with the CO_2 term as H_2CO_3* (Stumm & Morgan, 1981). While hydration and hydroxylation are both considered, they are not different reactions but kinetic pathways with different kinetic constants. Thus, the equilibrium state is not affected, but the time for the reaction is. Hydroxylation is also an important factor for high pH systems since the forward reaction dominates with HCO_3^- being produced (Stumm & Morgan, 1981).

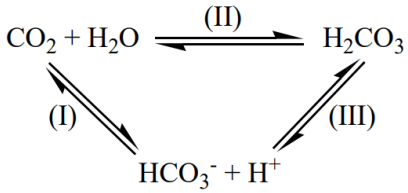

Figure 1.1: Reaction mechanism for hydration of CO_2

The pathways for protolysis and hydrolysis of HCO_3^- are shown in Figure 1.2 (Eigen et al., 1961; Watson et al., 2024). Path III represents the dissociation of water that connects the protolysis and hydrolysis pathways.

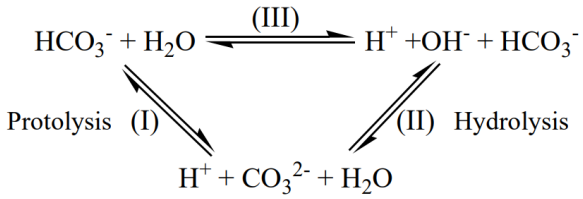

Figure 1.2: Reaction mechanism for protolysis and hydrolysis of HCO_3^-

Equilibrium constants can be defined for each equilibrium reaction, and then calculated. Kinetic constants are determined from literature review and tabulated for use in modeling of the carbonate system, in which the rate laws for each reaction mechanism can be derived.

While the enzyme, RuBisCO, starts the first reaction in carbon fixation by utilizing a CO_2 substrate, it has been hypothesized that algae have carbon concentrating mechanisms (CCMs) that allow for the use of HCO_3^- and CO_3^{2-} as substrates also (Patel et al., 1973; Zeebe & Gladrow, 2001; Cents et al., 2005). These CCMs are typically used in environments lacking in CO_2 to allow for high intracellular CO_2 concentration, where the process is carried out by a combination of active CO_2 pumps, HCO_3^- pumps, and/or external carbonic anhydrases (Patel et al., 1973; Cents et al., 2005). For freshwater green algae, it has been established that HCO_3^- can be used as a substrate for carbon fixation

through this mechanism, however, it is unclear whether CO_3^{2-} can be used in the same way. Especially in high pH systems greater than 10.3, CO_3^{2-} as an inorganic carbon source must be considered further since it is the dominant carbon species in alkaline systems.

Prior experiments have substantiated that freshwater algae continue to grow at pH as high as 11.5 (Watson & Drapcho, 2016; Watson et al., 2024). At the end of these open reactor experiments, TIC concentration exceeded the initial carbon provided despite algal consumption, which further proves greater carbon capture potential at high pH (Watson & Drapcho, 2016, Watson et al., 2024).

Enhanced Diffusion at High pH

For the purpose of modeling total inorganic carbon (TIC) in the system, atmospheric CO_2 diffusion will be considered for an open system, which is based on the two-film theory (Reichle et al., 1999). This model states diffusion of a molecule in gas phase to liquid phase occurs through a gas-liquid interface, where the overall mass transfer rate is impacted by the rate of diffusion from both phases on either side of the interface. A gas film exists from the gas phase to the interface, and a liquid film is formed from the interface to the liquid phase, giving rise to the 'two-film' label (Figure 1.3a). It is assumed that equilibrium exists at the interface, thus Henry's Law can be applied (Equation 1.2).

$$K_H = \frac{[CO_{2\,(aq)}]_{sat}}{p_{CO_2}} \qquad \text{(Equation 1.2)}$$

Where K_H = Henry's Law constant (Pa/M)
$[CO_{2\,(aq)}]_{sat}$ = equilibrium CO_2 concentration (M)
p_{CO_2}= CO_2 partial pressure (Pa)

For CO_2 diffusion, there is no significant mass transfer resistance in the gas film, so the overall mass transfer is determined by the resistance in the liquid film, which simplifies the model to a single boundary layer (Figure 1.3b) (NETL, 2008).

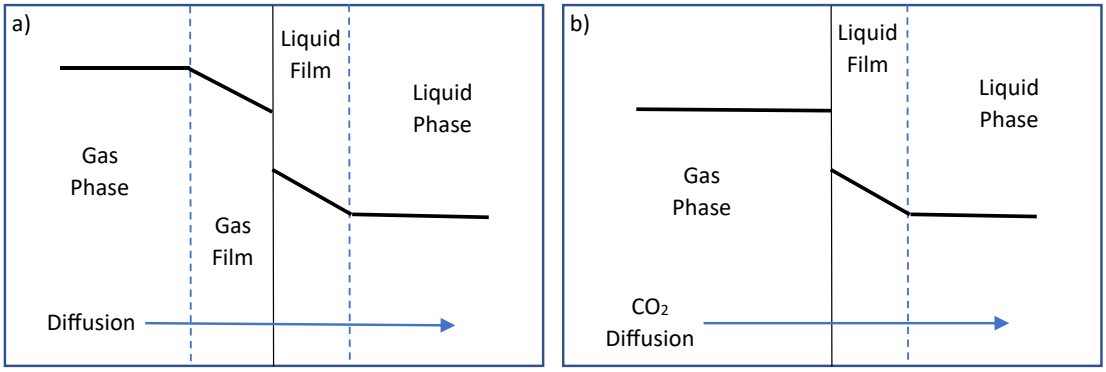

Figure 1.3: Panel a) shows a diagram of the two-film theory for general diffusion of a compound from gas to liquid phase. Panel b) shows a diagram of the two-film theory simplified for CO_2 diffusion, where there is no gas film mass transfer (NETL, 2008).

Three specific cases can be applied to determine the boundary layer mass transfer, which are important considerations for CO_2 diffusion: unenhanced diffusion, kinetic enhanced diffusion, and equilibrium enhanced diffusion. For unenhanced diffusion, no reactions occur in the boundary layer and mass transfer is based on Fick's Law (Equation 1.3), (Millero, 1995). The liquid diffusivity of CO_2 is dependent on temperature and can be determined with the Arrhenius equation given the Arrhenius constant for CO_2 (Stumm & Morgan, 1981).

$$\frac{d[CO_2]}{dt} = \frac{D_{CO_2} * a}{L} * [(CO_2)_{sat} - (CO_2)_{bulk}] \quad \text{(Equation 1.3)}$$

Where D_{CO_2}= liquid diffusivity of CO_2 (m^2/s)
L = boundary layer thickness (m)
a = reactor interfacial area (1/m)
$[(CO_2)_{sat} - (CO_2)_{bulk}]$ = CO_2 concentration difference between bulk liquid and the interface (kg/m^3)

However, CO_2 can stay in the boundary layer long enough for hydration, the conversion of aqueous CO_2 and subsequently H_2CO_3 into HCO_3^- in the presence of water, and hydroxylation, the conversion of aqueous CO_2 directly into HCO_3^- in the presence of hydroxide. This process allows for kinetically enhanced diffusion, in which case the reaction rates must also be applied to the transient mass balance expression (Equation 1.4) (NETL, 2008). These reactions lead to a concentration gradient in the boundary layer, with a higher CO_2 concentration at the interface.

$$\frac{d[CO_2]}{dt} = D_{CO_2} * \frac{\partial^2[CO_2]}{\partial z^2} + \left(\frac{\partial[CO_2]}{\partial t}\right)_{reaction} \quad \text{(Equation 1.4)}$$

In order to quantify the CO_2 conversion reaction rates, an enhanced TIC transport model is considered, where the pH varies as distance from the interface increases (Eigen et al., 1961; Millero, 1995). The resulting concentration gradients for the three inorganic carbon species, CO_2, HCO_3^-, and CO_2^{2-}, are used to determine the TIC flux, which is the sum of each species' flux (Eigen et al., 1961). Justified by the rapid diffusivity of H^+ ions, this model has been simplified with the assumption of constant pH, equivalent to the bulk liquid pH (Bolin, 1960; Hoover & Berkshire, 1969; NETL, 2008). This modified model also has issues since the assumption of constant pH ignores boundary layer electroneutrality (Eigen et al., 1961). The discrepancy can be addressed via an analytic

solution that removes the consideration of ionic diffusion by evaluating the flux at the interface. From the modified enhanced TIC model, the enhanced TIC flux is defined in terms of four related parameters: r, reacto-diffusive length (a_k), Damkohler number (Da), and enhancement factor (EF) (Edsall, 1969; NETL, 2008). The chemically enhanced TIC flux (F_e) is shown in Equation 1.6, which was developed from steady state conditions of hydration and hydroxylation in the boundary layer, and the assumptions that HCO_3^- is constant through the boundary layer and the pH in the boundary layer and bulk liquid are equivalent (NETL, 2008). The r-term is defined in Equation 1.5 (NETL, 2008).

$$r = \sqrt{\frac{k_+[H^+]+k_{+4}K_w}{D_{CO_2}[H^+]}} \qquad \text{(Equation 1.5)}$$

Where r = r-term (1/m)
k_+ = kinetic rate constant for forward reaction of CO_2 hydration (1/M-s)
k_{+4} = kinetic rate constant for forward reaction of CO_2 hydroxylation (1/M-s)
K_w = equilibrium constant for hydrolysis of water (M)
$[H^+]$ = hydrogen ion concentration in bulk liquid (M)
D_{CO_2} = liquid diffusivity of CO_2 (m^2/s)

$$F_e = D_{CO_2} * r * \frac{\cosh(r*L)}{\sinh(r*L)} * [(CO_2)_{sat} - (CO_2)_{bulk}] \qquad \text{(Equation 1.6)}$$

Where F_e = chemically enhanced TIC flux (kg/m^2-s)
D_{CO_2} = liquid diffusivity of CO_2 (m^2/s)
r = r-term (1/m)
L = boundary layer thickness (m)
$[(CO_2)_{sat} - (CO_2)_{bulk}]$ = CO_2 concentration difference between bulk liquid and the interface (kg/m^3)

The reacto-diffusive length (a_k) is a measure of the relative importance of diffusion and CO_2 reactions, which is based on the reaction rate constant (k), and the diffusivity (D), and is inversely related to r (Equation 1.7) (Edsall, 1969). It can be interpreted that the reactions in the boundary layer are less significant than diffusion

when the a_k is high; however, in open carbonate systems the a_k and r terms must also be compared to boundary layer thickness when discerning if diffusion or reaction rates limit CO_2 absorption.

$$a_k = \sqrt{\frac{D}{k}} = \sqrt{\frac{D_{CO_2}}{k_+ + k_{+4}[OH^-]}} = \frac{1}{r} \qquad \text{(Equation 1.7)}$$

Where a_k = reacto-diffusive length (m)
D = diffusivity (m^2/s)
k = kinetic rate constant for forward reaction of CO_2 hydration (1/s)
k_+ = kinetic rate constant for forward reaction of CO_2 hydration (1/s)
k_{+4} = kinetic rate constant for forward reaction of CO_2 hydroxylation (1/M-s)
$[OH^-]$ = hydroxide ion concentration in bulk liquid (M)
r = r-term (1/m)

The Damkohler number (Da) and the enhancement factor (EF) are analogous dimensionless mass transfer parameters that do consider the boundary layer thickness on the relative importance of diffusion and reactions (Equations 1.8 and 1.9). For small Da values significantly less than 1, diffusion is the controlling process for CO_2 absorption, while for Da values much greater than 1, reactions are the controlling process (Edsall, 1969). Similarly for large EF numbers, reactions dominate.

$$Da = \left(\frac{L}{a_k}\right)^2 = (L * r)^2 \qquad \text{(Equation 1.8)}$$

$$EF = \frac{F_e}{F} = r * L * \coth(r * L) = \frac{L}{a_k} * \coth\left(\frac{L}{a_k}\right) = \sqrt{Da} * \coth\left(\sqrt{Da}\right) \qquad \text{(Equation 1.9)}$$

Where Da = Damkohler number (unitless)
L = boundary layer thickness (m)
a_k = reacto-diffusive length (m)
r = r-term (1/m)
EF = enhancement factor (unitless)
F_e = chemically enhanced TIC flux (kg/m^2-s)
F = enhanced TIC flux (kg/m^2-s)

Maximizing the EF parameter results in equilibrium enhanced diffusion, the third case applied to determine the boundary layer mass transfer. This peak for kinetically enhanced diffusion is reached by forcing the reaction rates to approach infinity, allowing equilibrium in the boundary layer (Eigen et al., 1961; NETL, 2008). Shown in Equation 1.10, the ratio of free CO_2 to TIC in the boundary layer is evaluated under constant pH assumption (Bolin, 1960; NETL, 2008).

$$EF_{max} = \frac{[H^+]^2 + K_1[H^+]^2 + K_1K_2}{[H^+]^2} \qquad \text{(Equation 1.10)}$$

Where EF_{max} = maximum enhancement factor (unitless)
$[H^+]$ = hydrogen ion concentration in bulk liquid (M)
K_1 = equilibrium constant for CO_2 hydration (unitless)
K_2 = equilibrium constant for HCO_3^- hydrolysis (M^2)

At high pH for open carbonate systems, hydration of CO_2 to HCO_3^- occurs at much faster rates as the bicarbonate formed pushes the reaction forward to more CO_2 diffusion. High pH also indicates a lower hydrogen ion concentration, which results in a large enhancement factor value. Thus, systems at high pH allow for more carbon capture by algae growth through the greater diffusion of CO_2.

Conclusion

Global CO_2 emissions are rising despite well-documented research on the detrimental effects of high atmospheric CO_2, from average global temperature increases to ocean acidification. Thus, microalgal carbon capture research is necessary to provide sustainable solutions for carbon draw down on a large scale. Autotrophic freshwater green algae can utilize both TAN and NO_3-N and, through biological mechanisms,

provide a source of culture pH control. At high pH, CO_2 diffusion kinetics are enhanced to allow for more significant carbon drawdown, and potential interactions with NH_3 can result in even greater mass transfer. However, TAN toxicity and volatilization can cause challenges in designing and modeling cultivation systems. To help address these issues, the research presented in Chapter Two will determine whether TAN and NO_3-N utilization is sequential or simultaneous and quantify the effects of nitrogen source on culture pH and algal growth kinetic and stoichiometric parameters.

References

Abeliovich, A., & Azov, Y. (1976). Toxicity of ammonia to algae in sewage oxidation ponds. *Applied and Environmental Microbiology*, *31*(6), 801–806. https://doi.org/10.1128/aem.31.6.801-806.1976

Aslan, S., & Kapdan, I. K. (2006). Batch kinetics of nitrogen and phosphorus removal from synthetic wastewater by algae. *Ecological Engineering*, *28*(1), 64–70. https://doi.org/10.1016/j.ecoleng.2006.04.003

Azov, Y., & Goldman, J. C. (1982). Free ammonia inhibition of algal photosynthesis in intensive cultures. *Applied and Environmental Microbiology*, *43*(4), 735–739. https://doi.org/10.1128/aem.43.4.735-739.1982

Baldia, S. F., Nishijima, T., Hata, Y., & Fukami, K. (1991). Growth characteristics of a blue-green alga spirulina platensis for nitrogen utilization. *NIPPON SUISAN GAKKAISHI*, *57*(4), 645–654. https://doi.org/10.2331/suisan.57.645

Bohutskyi, P., Kligerman, D. C., Byers, N., Nasr, L. K., Cua, C., Chow, S., Su, C., Tang, Y., Betenbaugh, M. J., & Bouwer, E. J. (2016). Effects of inoculum size, light intensity, and dose of anaerobic digestion centrate on growth and productivity of Chlorella and scenedesmus microalgae and their poly-culture in primary and secondary wastewater. *Algal Research*, *19*, 278–290. https://doi.org/10.1016/j.algal.2016.09.010

Bolin, B. (1960). On the exchange of carbon dioxide between the atmosphere and the sea. *Tellus*, *12*(3), 274–281. https://doi.org/10.1111/j.2153-3490.1960.tb01311.x

Cents, A. H. G., Brilman, D. W. F., & Versteeg, G. F. (2005). CO2 absorption in carbonate/bicarbonate solutions: The Danckwerts-criterion revisited. *Chemical Engineering Science*, *60*(21), 5830–5835. https://doi.org/10.1016/j.ces.2005.05.020

Collos, Y., & Harrison, P. J. (2014). Acclimation and toxicity of high ammonium concentrations to unicellular algae. *Marine Pollution Bulletin*, *80*(1–2), 8–23. https://doi.org/10.1016/j.marpolbul.2014.01.006

Crofts, A. R. (1966). Uptake of ammonium ion by chloroplasts, and the mechanism of amine uncoupling. *Biochemical and Biophysical Research Communications*, *24*(1), 127–134. https://doi.org/10.1016/0006-291x(66)90420-7

Dalrymple, O. K., Halfhide, T., Udom, I., Gilles, B., Wolan, J., Zhang, Q., & Ergas, S. (2013). Wastewater use in algae production for generation of renewable resources: A review and preliminary results. *Aquatic Biosystems*, *9*(1), 2. https://doi.org/10.1186/2046-9063-9-2

Drapcho, C. M., Nhuan, N. P., & Walker, T. H. (2020). *Biofuels Engineering Process Technology*. McGraw-Hill.

Edsall, J.T. (1969). Carbon Dioxide, Carbonic Acid and Bicarbonate Ion: Physical Properties and Kinetics of Interconversion.

Eigen, M. (1964). Proton transfer, acid-base catalysis, and enzymatic hydrolysis. part I: Elementary processes. *Angewandte Chemie International Edition in English*, *3*(1), 1–19. https://doi.org/10.1002/anie.196400011

Eigen, M., Kustin, K., & Maass, G. (1961). Die geschwindigkeit der hydratation von *so* 2 in Wäßriger Lösung. *Zeitschrift Für Physikalische Chemie*, *30*(1_2), 130–136. https://doi.org/10.1524/zpch.1961.30.1_2.130

Eze, V. C., Velasquez-Orta, S. B., Hernández-García, A., Monje-Ramírez, I., & Orta-Ledesma, M. T. (2018). Kinetic modelling of microalgae cultivation for wastewater treatment and carbon dioxide sequestration. *Algal Research*, *32*, 131–141. https://doi.org/10.1016/j.algal.2018.03.015

Farrelly, D. J., Everard, C. D., Fagan, C. C., & McDonnell, K. P. (2013). Carbon sequestration and the role of Biological Carbon Mitigation: A Review. *Renewable and Sustainable Energy Reviews*, *21*, 712–727. https://doi.org/10.1016/j.rser.2012.12.038

Gutierrez, J., Kwan, T. A., Zimmerman, J. B., & Peccia, J. (2016). Ammonia inhibition in oleaginous microalgae. *Algal Research*, *19*, 123–127. https://doi.org/10.1016/j.algal.2016.07.016

Hoover, T. E., & Berkshire, D. C. (1969). Effects of hydration on carbon dioxide exchange across an air-water interface. *Journal of Geophysical Research*, *74*(2), 456–464. https://doi.org/10.1029/jb074i002p00456

IEA (2024), CO2 Emissions in 2023, IEA, Paris https://www.iea.org/reports/co2-emissions-in-2023, Licence: CC BY 4.0

Ip, S. Y., Bridger, J. S., Chin, C. T., Martin, W. R. B., & Raper, W. G. C. (1982). Algal growth in primary settled sewage. *Water Research*, *16*(5), 621–632. https://doi.org/10.1016/0043-1354(82)90083-5

Kumar, A., & Bera, S. (2020). Revisiting nitrogen utilization in Algae: A review on the process of regulation and assimilation. *Bioresource Technology Reports*, *12*, 100584. https://doi.org/10.1016/j.biteb.2020.100584

Lachmann, S. C., Mettler-Altmann, T., Wacker, A., & Spijkerman, E. (2019). Nitrate or ammonium: Influences of nitrogen source on the physiology of a green alga. *Ecology and Evolution*, *9*(3), 1070–1082. https://doi.org/10.1002/ece3.4790

Lu, Q., Chen, P., Addy, M., Zhang, R., Deng, X., Ma, Y., Cheng, Y., Hussain, F., Chen, C., Liu, Y., & Ruan, R. (2018). Carbon-dependent alleviation of ammonia toxicity for algae cultivation and associated mechanisms exploration. *Bioresource Technology*, *249*, 99–107. https://doi.org/10.1016/j.biortech.2017.09.175

Maestrini, S. Y., Robert, J.-M., Leftley, J. W., & Collos, Y. (1986). Ammonium thresholds for simultaneous uptake of ammonium and nitrate by oyster-pond algae. *Journal of Experimental Marine Biology and Ecology*, *102*(1), 75–98. https://doi.org/10.1016/0022-0981(86)90127-9

Markou, G., Depraetere, O., & Muylaert, K. (2016). Effect of ammonia on the photosynthetic activity of Arthrospira and chlorella: A study on chlorophyll fluorescence and Electron Transport. *Algal Research*, *16*, 449–457. https://doi.org/10.1016/j.algal.2016.03.039

Maryshamya, A., Rajasekar, T., & Rengasamy, R. (2019). Carbon sequestration potential of scenedesmus quadricauda (Turpin) and evaluation on zebra fish (Danio rerio). *Aquaculture Reports*, *13*, 100178. https://doi.org/10.1016/j.aqrep.2018.100178

Millero, F. J. (1995). Thermodynamics of the carbon dioxide system in the oceans. *Geochimica et Cosmochimica Acta*, *59*(4), 661–677. https://doi.org/10.1016/0016-7037(94)00354-o

Moeller, M. B., & Vlek, P. L. G. (1982). The chemical dynamics of Ammonia volatilization from aqueous solution. *Atmospheric Environment (1967)*, *16*(4), 709–717. https://doi.org/10.1016/0004-6981(82)90388-2

Morales-Amaral, M. del, Gómez-Serrano, C., Acién, F. G., Fernández-Sevilla, J. M., & Molina-Grima, E. (2015). Outdoor production of scenedesmus sp. in thin-layer and raceway reactors using centrate from anaerobic digestion as the sole nutrient source. *Algal Research*, *12*, 99–108. https://doi.org/10.1016/j.algal.2015.08.020

NETL, Carbon Sequestration Atlas of the United States and Canada (2008).

Padil, Putra, M. D., Nata, I. F., Wicakso, D. R., Zulfarina, Irawan, C., & Sunarno. (2023). Microalgae growth kinetic study with logistic and Monod Models. *AIP Conference Proceedings*. https://doi.org/10.1063/5.0131575

Park, J., Jin, H.-F., Lim, B.-R., Park, K.-Y., & Lee, K. (2010). Ammonia removal from anaerobic digestion effluent of livestock waste using green alga scenedesmus SP.. *Bioresource Technology*, *101*(22), 8649–8657. https://doi.org/10.1016/j.biortech.2010.06.142

Patel, R. C., Boe, R. J., & Atkinson, G. (1973). The CO2-water system. I. Study of the slower hydration-dehydration step. *Journal of Solution Chemistry*, *2*(4), 357–372. https://doi.org/10.1007/bf00713250

Qin, F., Wang, S., Hartono, A., Svendsen, H. F., & Chen, C. (2010). Kinetics of CO2 absorption in aqueous ammonia solution. *International Journal of Greenhouse Gas Control*, *4*(5), 729–738. https://doi.org/10.1016/j.ijggc.2010.04.010

Reichle, D., Houghton, J., Kane, B., Ekmann, J., & and others. (1999). *Carbon Sequestration Research and Development*. https://doi.org/10.2172/810722

Ribita, D. (2011). (thesis). *Quantification of scenedesmus dimorphus growth and substrate kinetics for continuous photobioreactor design*. Cleveland State University, Cleveland, OH.

Sanz-Luque, E., Chamizo-Ampudia, A., Llamas, A., Galvan, A., & Fernandez, E. (2015). Understanding nitrate assimilation and its regulation in microalgae. *Frontiers in Plant Science*, *6*. https://doi.org/10.3389/fpls.2015.00899

Sousa, C. A., Sousa, H., Vale, F., & Simões, M. (2021). Microalgae-based bioremediation of wastewaters - influencing parameters and mathematical growth modelling. *Chemical Engineering Journal*, *425*, 131412. https://doi.org/10.1016/j.cej.2021.131412

Stumm, W., & Morgan, J. J. (1981). *Aquatic chemistry: An introd. emphasizing chemical equilibria in natural waters*. Wiley.

Wang, X., Conway, W., Fernandes, D., Lawrance, G., Burns, R., Puxty, G., & Maeder, M. (2011). Kinetics of the reversible reaction of CO2(AQ) with ammonia in aqueous solution. *The Journal of Physical Chemistry A*, *115*(24), 6405–6412. https://doi.org/10.1021/jp108491a

Watson, M. K., & Drapcho, C. M. (2016). Kinetics of inorganic carbon-limited freshwater algal growth at high ph. Transactions of the ASABE, 59(6), 1633–1643. https://doi.org/10.13031/trans.59.11520

Watson, M. K., Flanagan, E., & Drapcho, C. M. (2024). Inorganic carbon-limited freshwater algal growth at high pH: revised with focus on alkalinity. Manuscript in preparation.

Xin, L., Hong-ying, H., Ke, G., & Ying-xue, S. (2010). Effects of different nitrogen and phosphorus concentrations on the growth, nutrient uptake, and lipid accumulation of a freshwater microalga scenedesmus sp.. *Bioresource Technology*, *101*(14), 5494–5500. https://doi.org/10.1016/j.biortech.2010.02.016

Zeebe, R. E., & Wolf-Gladrow, D. A. (2001). *Cob2s in seawater: Equilibrium, Kinetics, isotopes*. Elsevier.

CHAPTER TWO

IMPACT OF NITROGEN SPECIES ON ALGAL GROWTH

Abstract

The objectives of this study are to quantify the effects of nitrate nitrogen (NO_3-N) and total ammonia nitrogen (TAN) as single and mixed nitrogen sources on freshwater autotrophic algal growth kinetic and stoichiometric parameters and culture pH, and to identify nitrogen uptake as simultaneous or sequential. Five reactors with varying ratios of NO_3-N and TAN in modified BG11 medium with no added inorganic carbon were inoculated with *Scenedesmus* sp., adjusted initially to 10.3 pH, left open to the atmosphere under low indoor light conditions, and monitored for a month. The following parameters were monitored daily: pH, light intensity, temperature, optical density (OD), total inorganic carbon (TIC), TAN, and NO_3-N concentrations. Specific growth rates were analyzed based on three identified phases of growth: phase one with likely no carbon limitation and TAN utilization, phase two with carbon limitation and TAN utilization, and phase three with carbon limitation and NO_3-N utilization. The highest specific growth rates were observed during phase one, which was not impacted by initial TAN concentration. The average specific growth rate during phase one was calculated as 0.043 hr^{-1}. Phase two specific growth rates were likely impacted by TAN but were not statistically significant, while phase three specific growth rates were statistically impacted by initial NO_3-N. Biomass yields on a nitrogen basis were assessed based on periods of TAN or NO_3-N use. In reactors containing both nitrogen sources, TAN was utilized preferentially by the algae with NO_3-N utilization after TAN depletion. The

culture pH was stable during TAN consumption and rose once NO_3-N was utilized; the greatest pH for the largest TAN:NO_3-N ratio was 10.990, while the greatest pH for the NO_3-N only treatment was 11.319. The design of algal cultivation systems for carbon capture can be informed by this study's results, especially the application of NO_3-N and TAN as biological pH control to provide conditions conducive to both carbon capture and algal growth.

Introduction

With global carbon emissions persistently rising despite the threat of 1.5^{o}C warming by the early 2030s, removing excess atmospheric carbon dioxide (CO_2) should be considered as a strategy to mitigate the complex ecological and social effects of climate change (Lee et al., 2021). Technological carbon capture methods, through chemical or physical means, have been criticized for being ineffective, energy-intensive, and financially demanding; however, biological carbon capture with microalgae can address these concerns while providing a sustainable biomass source for high-value algal products (Farrelly et al., 2013). The autotrophic metabolic pathway of algal carbon fixation has been well established, but research on maximizing carbon uptake via enhanced atmospheric CO_2 diffusion at high pH with various nitrogen sources is lacking. BG11 algal growth medium provides nitrate nitrogen (NO_3-N) as the nitrogen source, though it is hypothesized that freshwater green algae prefer total ammonia nitrogen (TAN) since no reduction is required for nitrogen assimilation (Sanz-Luque et al., 2015; Lachmann et al., 2019). Microalgae can utilize both TAN and NO_3-N for nitrogen

assimilation, making them substitutable substrates (Drapcho et al., 2020). In environments where both TAN and NO_3-N sources are available, utilization can be classified as sequential or simultaneous; an identification is necessary for accurate Monod algal growth modeling.

Through autotrophic growth, algae consume inorganic carbon, along with other essential nutrients, such as nitrogen, to produce biomass and oxygen. Algae can benefit from enhanced carbon dioxide diffusion kinetics at high pH, resulting in up to 90% capturing efficiency in open systems (Sayre, 2010). Theoretically according to Redfield ratios, 2.79 grams of biomass can be produced for every gram of CO_2 consumed, with experimental observations indicating up to 2.91-2.86 g of biomass per g of carbon in open reactors for a range of 0.05-0.20 g/L initial Na_2CO_3 treatments (Watson et al., 2024). Biomass yields can be maximized for inorganic carbon-based algal growth by establishing the preferred nitrogen source, which can also provide a means of pH control in algal carbon capture systems. Autotrophic algal growth with a NO_3-N consumes H^+ ions and raises the pH, and TAN use produces H^+ ions and lowers the pH (Markou et al., 2016). Equations 2.1 and 2.2, developed by Watson et al. (2024), show the balanced chemical equations for autotrophic algal growth based on Redfield ratios for biomass, a CO_2 inorganic carbon substrate, and TAN or NO_3-N as the nitrogen source, respectively.

$$106CO_2 + 16NO_3^- + HPO_4^{2-} + 18H^+ + 122H_2O \xrightarrow{photosynthesis} C_{106}H_{263}O_{110}N_{16}P + 138O_2 \quad \text{(Equation 2.1)}$$

$$106CO_2 + 16NH_4^+ + HPO_4^{2-} + 108H_2O \xrightarrow{photosynthesis} C_{106}H_{263}O_{110}N_{16}P + 107O_2 + 14H^+ \quad \text{(Equation 2.2)}$$

However, TAN is also toxic to microalgae, causing inhibition of photosynthesis via amine uncoupling in chloroplasts and preventing growth at high concentrations

(Crofts, 1966; Azov & Goldman, 1982). Larger TAN concentrations cause greater inhibition and tolerance is dependent on algal species and ammoniacal nitrogen form, with Abeliovich & Azov (1976) finding total growth inhibition for *Scenedesmus obliquus* at 3 mM ammonia nitrogen (NH_3-N). Both forms of TAN, NH_3 and NH_4^+, have toxic effects, but NH_3 is more inhibitive as being gaseous, uncharged, and lipid-soluble allows free diffusion across the cell membrane (Collos & Harrison, 2014). The dominant form of TAN, and so the severity of toxicity effects, is heavily influenced by pH, where pH greater than dissociation constant (pK_a) of 9.25 shifts the equilibrium to NH_3 (Markou et al., 2016). In algal reactors with mixed nitrogen sources and changing pH over time, determining inhibition levels and modeling becomes more complex.

Thus, research of carbon capture technology through algae cultivation is essential, not as a single solution to solve the climate crisis and allow for further reckless emissions, but to help draw down carbon and to provide sustainable sources of algal biomass for high-value materials that could lead to carbon sequestration. The goal of this research was to explore the impact of nitrogen species on carbon abatement by a green freshwater alga. The following objectives will be accomplished:

i. Identify nitrogen uptake preference as simultaneous or sequential in cultures with mixed nitrogen sources.

ii. Quantify the effect of NO_3-N and TAN as single and mixed nitrogen sources on culture pH.

iii. Quantify the effect of NO_3-N and TAN as single and mixed nitrogen sources on kinetic and stoichiometric growth parameters.

Materials and Methods

Experimental Design

Five glass reactors of four-liter liquid volume were each prepared with modified BG11 growth medium (Table 2.1) initially adjusted to 10.3 pH using a 5 M NaOH solution. The reactors were open to the atmosphere to allow for CO_2 diffusion and had no external inorganic carbon supplementation. The five nitrogen treatments consisted of varying ratios of TAN and NO_3-N (Table 2.2) with a total nitrogen concentration of 2 mM. Though the standard concentration of NO_3-N in BG11 growth medium is 17.6 mM, based on preliminary experimentation and literature review (Chapter One), an equivalent concentration in TAN at 10.3 pH completely inhibits algal growth. According to Abeliovich & Azov (1976) for *Scenedesmus obliquus* cultures, TAN inhibition begins at 2 mM NH_3-N at pH greater than 8.0, and growth is totally inhibited at 3 mM NH_3-N. Thus, the total nitrogen in all reactor treatments was set at 2 mM.

Table 2.1: Modified BG11 growth medium used in study (0.02 g Na_2CO_3 omitted)

Chemical	Concentration (g/L)
K_2HPO_4	0.04
$MgSO_4$ $7H_2O$	0.075
$CaCl_2$ $2H_2O$	0.036
Citric acid	0.006
Ferric ammonium citrate	0.006
EDTA	0.001
A5 Trace Metal Mix	1.0 mL/L of solution
A5 Trace Metal Mix:	
H_3BO_3	2.86
$MnCl_2$ $4H_2O$	1.81
$ZnSO_4$ $7H_2O$	0.222
Na_2MoO_4 $2H_2O$	0.39

$CuSO_4$ $5H_2O$	0.079
$Co(NO_3)_2$ $6H_2O$	0.0494 mg/L

Table 2.2: Nitrogen Treatments

TAN Concentration	**NO_3-N Concentration**
1.00 mM (53.49 mg NH_4Cl/L)	1.00 mM (84.99 mg $NaNO_3$/L)
0.75 mM (40.12 mg NH_4Cl/L)	1.25 mM (106.24 mg $NaNO_3$/L)
0.50 mM (26.75 mg NH_4Cl/L)	1.50 mM (127.49 mg $NaNO_3$/L)
0.25 mM (13.37 mg NH_4Cl/L)	1.75 mM (148.74 mg $NaNO_3$/L)
0.00 mM	2.00 mM (169.99 mg $NaNO_3$/L)

The five reactors were randomly assigned a position under continuous artificial lighting with a mix of cool white F20 and F48 – high output bulbs, which produced approximately 100 µmol/m^2*s in the photosynthetically active radiation (PAR) range at the reactor liquid surface (Figure 2.1). The ambient air temperature was maintained at 21^{o}C. The reactors were mixed at 150 rpm with 3.125 in magnetic stir bars. Due to an initial error with the 0.75 mM TAN, 1.75 mM NO_3-N reactor, the reactor was initiated and inoculated three days after the other reactors began growing.

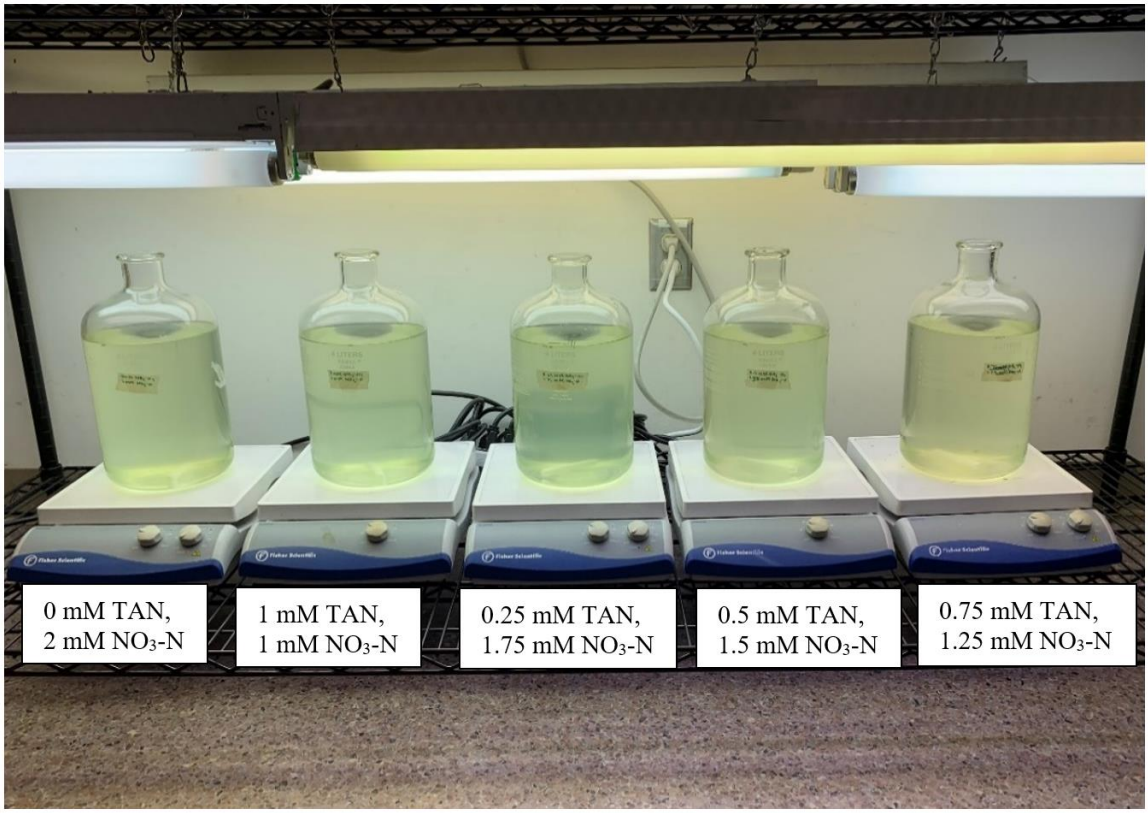

Figure 2.1: Reactor setup

Algal Culture

A pure *Scenedesmus* sp. inoculum (Carolina Biological Supply, Item #152510) was cultured in modified BG11 medium with a mixed nitrogen treatment (0.50 mM TAN and 1.50 mM NO_3-N**)** and initial pH of 10.3 to acclimate the algae to a low carbon, high pH environment with ammonia presence. The preculture was monitored for a week to ensure successful growth in the experimental environment and provide a robust inoculum. Each four-liter working volume was inoculated with 16 mg of algae from the preculture for an initial 4 mg/L algal biomass concentration.

Data Collection and Analysis

The following parameters were monitored daily for the first ten days and then with various frequencies for a total of 30 days: light, temperature, optical density (OD) at 750 nm, pH, total inorganic carbon (TIC), TAN, and NO_3-N concentrations. Water loss from evaporation between sampling periods was replenished by marking the liquid level after sample collection and filling with deionized, distilled (DDI) water to the marked line before the following collection. The total volume removed from each reactor for analysis was 135 mL per sampling period if all assays were being performed. Except for OD, the total sample volume was vacuum filtered with 0.2 µm nylon membrane filters (Pall Corporation Nylaflo™ Nylon Membrane Disc Filter) before any analysis. Replicate measurements were recorded and averaged for all data, excluding light and reactor liquid temperature.

Light

Light intensities were quantified by PAR measurements using a Phantom PHOTOBIO Advanced Quantum PAR Meter. The PAR range was specified as the wavelengths of visible light between 400 and 700 nm. Four measurements were taken at the liquid surface level, flush to the outside of the vessel at the north, south, east, and west points, then averaged.

Temperature

The liquid temperature in the reactors was measured with a Thermo Scientific Orion Stainless-Steel Automatic Temperature Compensation (ATC) probe and Orion Dual Star pH/ISE Benchtop Meter. The liquid temperature of each TAN sample was also recorded during measurement for potential temperature corrections for ammonia volatilization during sampling, but later experimentation revealed this was not necessary (Appendix A).

Optical Density and Total Suspended Solids

OD was measured at 750 nm using a Thermo Scientific SPECTRONIC 200 spectrophotometer, calibrated with DDI water as the blank. A standard curve relating OD to Total Suspended Solids (TSS) concentration was created for each reactor treatment, following the membrane filter method described in Method 8111 G (APHA, 1995). The standard curves in Appendix E were generated from algal cells grown after experimentation and collected after 15 days of growth, which were concentrated with centrifugation. Samples were diluted if the measured OD was greater than 1.2, after which linearity between OD and TSS is not guaranteed. Actual OD was calculated by multiplying the diluted OD by the dilution factor.

pH

The pH of each sample was measured with a VWR Universal SJ 113 pH Electrode and Thermo Scientific Orion Dual Star pH/ISE Benchtop Meter, calibrated

with VWR pH Reference Standard Buffers, pH 4.00, 7.00, and 10.00, prior to sample measurement.

Total Inorganic Carbon (TIC)

TIC concentration was measured with a Shimadzu TOC-L Series Carbon Analyzer, which operated under measurement conditions listed in Table 2.3. Samples were stored in 25 mL glass vials, sealed with Parafilm to minimize CO_2 diffusion during handling, and immediately processed with the analyzer. A new calibration curve was produced with fresh standard solutions for each sample run. Five standard solutions of 0, 12.5, 25, 37.5, and 50 mg C/L were prepared via parallel dilutions of a 50/50 mix of Na_2CO_3 and $NaHCO_3$ stock solution.

Table 2.3: Parameters for Shimadzu TOC-L Series Analyzer Equipment

Analyzer Model	Shimadzu Model TOC-L Total Organic Carbon/Total Nitrogen Analyzer, with Model ASI-L autosampler
Measurement Method	Inorganic Carbon (IC), detection of CO_2 after phosphoric acid acidification of sample
Calibration Curve	Linear regression, zero shift, 50/50 mix Na_2CO_3 and $NaHCO_3$ standard concentrations: 0, 12.5, 25, 37.5, and 50 mg C/L
Injection Volume	50 µL
Standard Deviation (SD) Max	0.1
Coefficient of Variation (CV) Max	2
Number of Injections	3/5
Number of Washes	2

Total Ammonia Nitrogen

TAN concentration was measured with a Thermo Scientific Orion High-Performance Ammonia Electrode and Thermo Scientific Orion Dual Star pH/ISE Benchtop Meter. The electrode membrane was replaced weekly, and the electrode operation was checked before sample measurement following the electrode user guide method (Thermo Scientific, 2010). Between sample measurements, the electrode was stored in a 1 ppm TAN standard solution with 1 mL alkaline reagent (Cat. No. 951011). For overnight storage, the electrode was stored in the ammonia electrode storage solution (Cat. No. 951213). A direct calibration method using the meter in millivolt mode was utilized for measurement per the electrode manual, and a fresh stock solution for calibration standard preparation was made every two days and stored in the refrigerator (Thermo Scientific, 2010). A pH-adjusting ionic strength adjuster (ISA) solution was added to samples and standards and mixed for ~2 minutes before measurement. The addition of ISA established a similar ionic strength across all samples and standards and raised the pH to an 11-14 range to convert all ammonium to ammonia. Electrode calibration standards and sample preparation depended on the expected TAN concentration:

a. Low TAN concentration (≤1 ppm TAN) – Three standard solutions for electrode calibration were prepared by serial dilution of a stock solution prepared with NH_4Cl. The standard concentration levels were 0.01, 0.1, and 1 mg N/L. A 1:50 v/v ratio of low-level pH-adjusting ISA (Cat. No. 951210) was added before measurement.

b. High TAN concentration (≥1 ppm TAN) - Five standard solutions for electrode calibration were prepared by serial dilution of a stock solution prepared with NH_4Cl. The standard concentration levels were 1.25, 2.5, 5, 10, and 20 mg N/L. A 1:50 ratio of pH-adjusting ISA (Cat. No. 951211) volume to sample volume was added before measurement.

Nitrate Nitrogen

NO_3-N concentration was determined with a Thermo Scientific Dionex Aquion Ion Chromatography System with a Dionex ICS Series AS-DV Autosampler. A Dionex IonPac AS23-4µm anion analytical column and Dionex IonPac AG23-4µm guard were used in the analysis, with a prepared 954 mg $NaCO_3$/L eluent solution that had been degassed for one hour before use. The ion chromatograph was set with a 0.5 mL/min sample flow rate and a 27-minute sample run time, optimized for NO_3^- peak selection with preliminary experimentation (Appendix B). Prior tests also showed that a maximum 8 mg/L NO_3^- concentration prevented column overload and anion peak overlap; thus, all samples were diluted to approximately the 8 ppm NO_3^- level by a four-fold dilution initially (Appendix B). The number of dilutions needed was adjusted based on the previous sample measurement; as algae grew and consumed NO_3^-, less dilution was needed. The actual NO_3^- concentration was calculated by multiplying the peak area by the dilution factor to account for the dilutions. Each sample was double filtered using vacuum and syringe filtration with 0.2 µm filter membranes to prevent equipment damage from clogging. In order to construct a calibration curve, fresh standards were

prepared for each operation of the ion chromatograph using RICCA VeriSpec 1000 ppm NO_3^- standard for ion chromatography. With parallel dilutions for 15 and 7.5 mg NO_3^-/L standards and serial dilutions for the remainder, the standard level concentrations were 0.15625, 0.3125, 0.625, 1.25, 2.5, 5, 7.5, 10, 15, and 20 mg NO_3^-/L.

Cell Composition and Algal Growth Stoichiometry

After 30 days of data collection, new reactors were started with the same experimental setup and conditions to produce algal cells for cell composition analysis. Biomass was collected after 15 days of growth, during the exponential growth phase, and sent to Clemson University Agricultural Services Laboratory. Elemental carbon and nitrogen analysis was conducted with a Leco Combustion Analyzer, and phosphorous and other trace elements were determined using a Spectro ACROS ICP. For ICP solid samples, a wet ashing procedure with HNO_3+30%H_2O_2 was used for digestion before analyzation (*Wet ashing procedure*, n.d.). The results were used to calculate algal biomass C:N:P ratios and molecular weight.

Algal Growth Kinetic Analysis

The specific growth rate quantification for each reactor was characterized by three distinct phases of growth based on the availability of inorganic carbon and nitrogen source. A linear regression of the natural log of the biomass concentration vs time was plotted for each exponential growth phase, where the slope is the specific growth rate (Drapcho et al., 2020). The coefficient of determination was also reported for each linear

regression. IBM SPSS Statistics Version 27.0 software was used to analyze if the effects of nitrogen treatment on growth rates were statistically significant within the same growth phases (IBM Corp, 2020). Laerd Statistics was used as a resource for reporting and formatting statistical conclusions (Laerd Statistics, 2015).

The biomass yield was categorized by period of TAN or NO_3-N utilization, where biomass yield on a nitrogen basis is determined from the mass of cells produced per mass of nitrogen substrate utilized (Drapcho et al., 2020). The coefficient of determination was also reported for each linear regression. IBM SPSS Statistics Version 27.0 software was used to analyze if the effects of nitrogen treatment on biomass yield were statistically significant within the same period of nitrogen utilization (IBM Corp, 2020). Laerd Statistics was used as a resource for reporting and formatting statistical conclusions (Laerd Statistics, 2015).

Results and Discussion

Algal Growth and Substrate Utilization

Total Suspended Solids

Each reactor followed typical batch growth with an initial lag, exponential growth, and then the beginning of a stationary phase; however, a pronounced death phase was not observed by 700 hours despite all nitrogen being depleted before 500 hours in all reactors (Figure 2.2). After 500 hours, substantial growth was still observed in all reactors. Biomass concentration was similar between reactor treatments at first but started to deviate around 145-hours. Peak biomass concentrations on a dry weight basis were

712.1, 731.4, 650.0, 841.0, and 851.5 mg/L, respectively in the 1:1, 0.75:1.25, 0.5:1.5, 0.25:1.75, and 0:2 (TAN:NO_3-N) treatments. The NO_3-N only reactor consistently produced the greatest TSS concentration throughout growth.

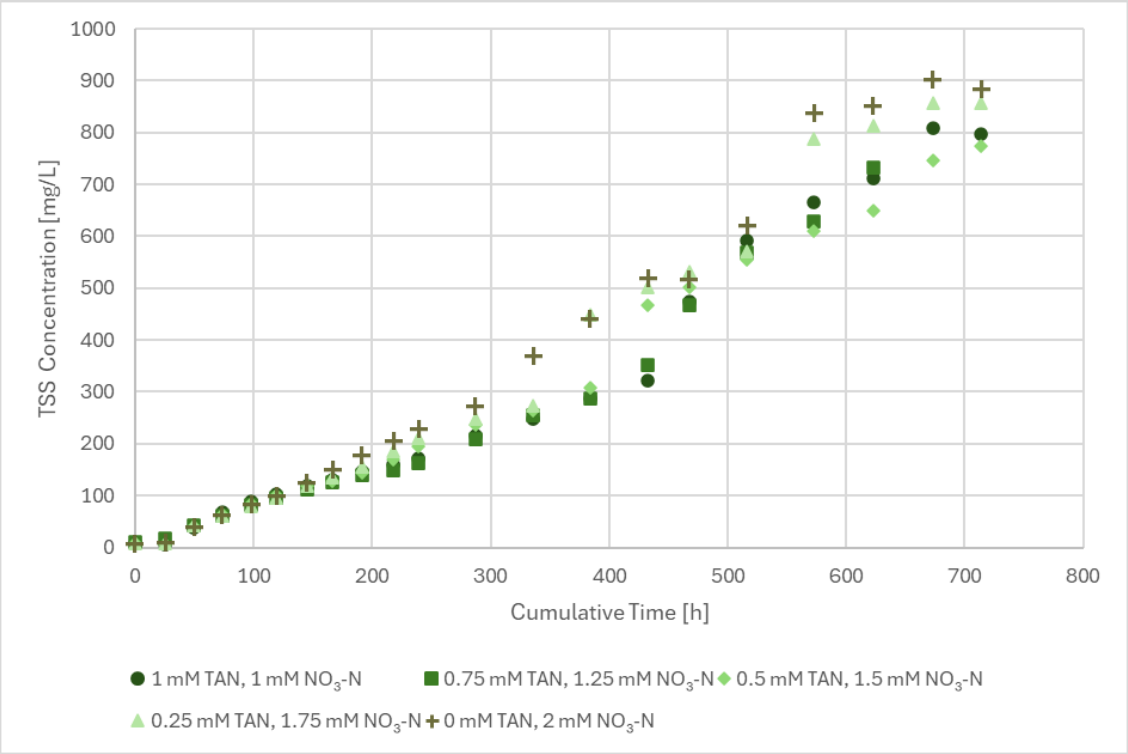

Figure 2.2: TSS concentration over time for the five nitrogen treatments

Inorganic Carbon

An initial peak in TIC was observed in all reactors at around 25.5 hours (Figure 2.3), likely due to CO_2 diffusion and low CO_2 uptake due to low initial biomass production. The initial peaks in TIC ranged from 1.9 to 2.7 mg/L C across reactors, which are expected to have physical/biological significance despite being relatively low concentrations. As the initial peaks were on par with the half-saturation constant for TIC for *Scenedesmus* of 4.9 mg/L C (Watson et al, 2024), it is further expected that carbon was not initially limiting in reactors. Indeed, the initial TIC peaks coincide with a steep

increase in the linearized biomass concentration after the first two initial lag points. Subsequently, natural log of the biomass begins to flatten after the initial TIC peak, which cannot be attributed to any TAN toxicity effects, since the NO_3-N only reactor follows this same pattern. In summary, carbon was unlikely to have been limiting until after 73.5 hours of growth.

Some smaller peaks in TIC were later observed. While there could be a biological mechanism of oscillatory TIC utilization, the smaller peaks of approximately 1 mg/L C are within the error associated with use of the carbon analyzer at higher experimental pH (Todd et al., 2024).

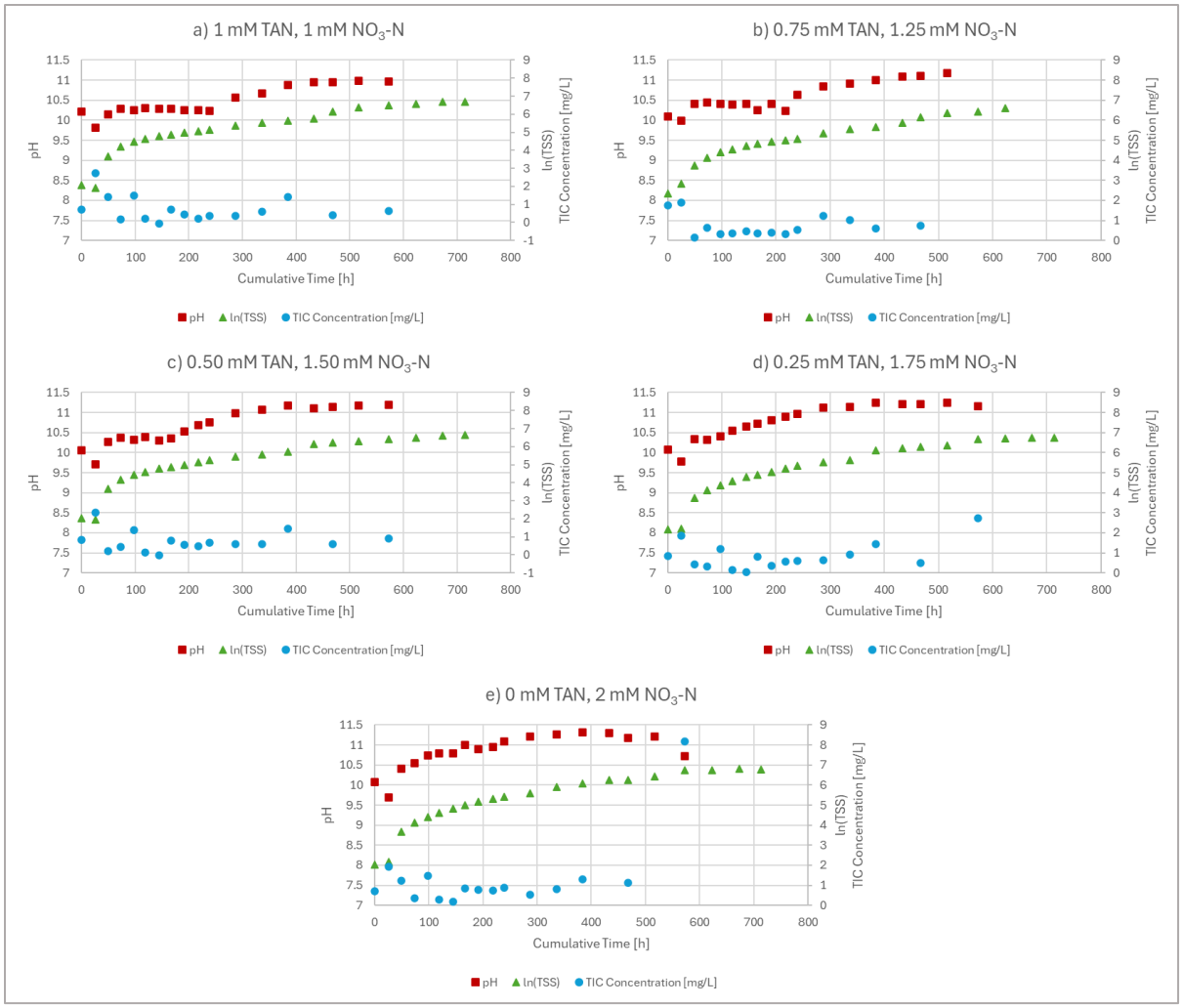

Figure 2.3: pH, TIC concentration, and natural log of biomass over time, with each reactor plotted in separate panels with letter designation a) through e)

Nitrogen

Nitrogen utilization was prominently sequential in reactors with mixed nitrogen sources. TAN consumption, shown in Figure 2.6a, began immediately as concentration continually declined until depletion, which occurred more quickly for lower initial TAN concentrations. For the greatest initial TAN concentration of 1 mM, depletion occurred around 239 hours and at 73.5 hours for the lowest concentration of 0.25 mM initial TAN. During the same period of TAN decline, NO_3-N concentration remained relatively stable

(Figure 2.6b). Only after TAN was completely exhausted did initial NO_3-N levels decrease. TAN utilization is considered to be the preferred substrate as it is less energy intensive in algal cells since the nitrogen is at the oxidation state (-III) required for amino acid synthesis (Sanz-Luque et al., 2015; Lachmann et al., 2019). TAN was probably used first in reactors where both nitrogen sources were available because at pH greater than the NH_4^+/NH_3 pK_a of 9.25, which was the case for all reactors for the entire experiment duration, the dominant form of TAN is gaseous NH_3 (Markou et al., 2016). NO_3-N and NH_4^+ cellular uptake is regulated at the membrane by transport enzymes, whereas gaseous NH_3 can freely diffuse into the cell (Sanz-Luque et al., 2015; Markou et al., 2016).

All nitrogen sources were depleted by 500 hours, yet from 500 to approximately 700 hours, appreciable growth was still observed (Figure 2.2). This phenomenon could indicate a mechanism of nitrogen accumulation, in which excess consumed nitrogen is either stored in inorganic forms or quickly converted to storage molecules in the form of protein or chlorophyll (Adams & Bugbee, 2014). One study found substantial chlorophyll molecule production and accumulation with excess extracellular nitrogen conditions followed by a rapid decline of chlorophyll cell content as external nitrogen was depleted (Li et al., 2008). Chlorophyll being used as an internal nitrogen store aligns with an observed color change in this experiment's reactors from bright green to yellowish during continued growth after nitrogen depletion (Figures 2.4 and 2.5).

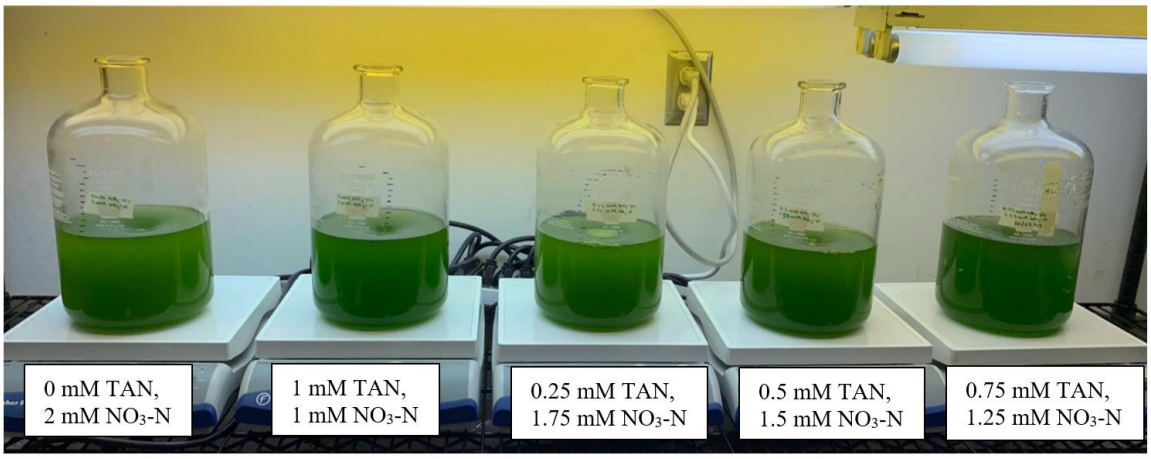

Figure 2.4: Reactors at 467.5 hours, near total nitrogen depletion

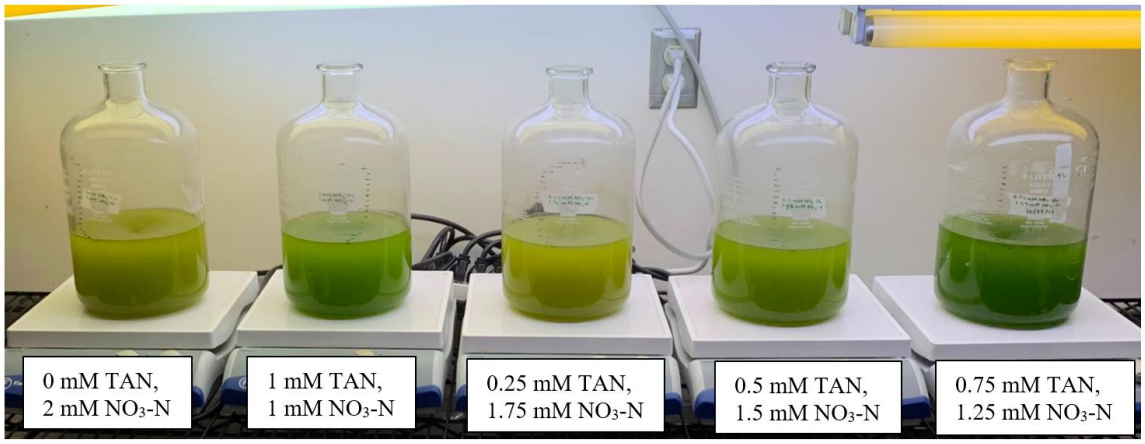

Figure 2.5: Reactors at 714 hours, well after total nitrogen depletion

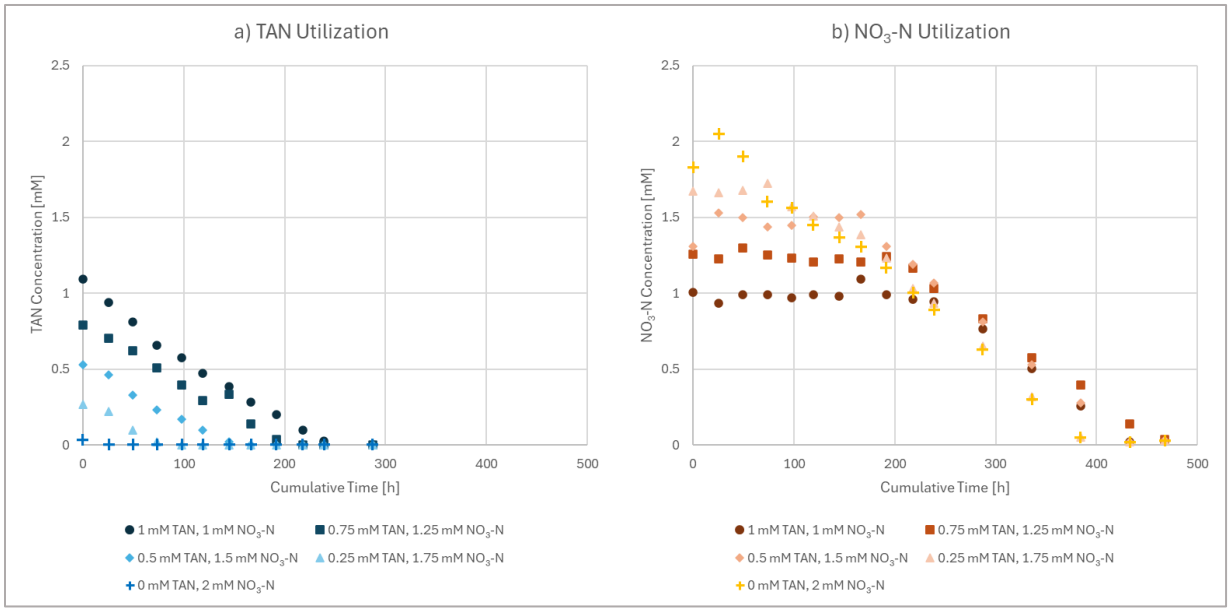

Figure 2.6: Nitrogen utilization over time for each reactor, with TAN and NO_3-N plotted in separate panels with letter designation a) and b), respectively

Three Distinct Growth Phases

Due to carbon changing from replete to limiting during the TAN utilization period and TAN/NO_3-N utilization occurring at different time intervals between reactors, algal growth was analyzed in three distinct phases (Table 2.4). Phase one occurred within the first 73.5 hours of growth and is classified as having the fastest specific growth rates. Only TAN is utilized during phase one in all reactors, except for the NO_3-N only treatment. Phase two is also distinguished by only TAN utilization, in addition to carbon limitation, with an apparent reduction in specific growth rates as biomass increased and the carbon consumption rate exceeded carbon diffusion rate into the system. The second phase for all reactors began around 73.5-hr, but ended at different periods depending on when TAN was totally depleted. Phase three is categorized by NO_3-N utilization, limited carbon, and the slowest specific growth rates.

There is no phase two growth for the 0.25 mM TAN, 1.25 mM NO_3-N treatment because all TAN is utilized in the first phase, with no carbon limitation. For the NO_3-N only reactor, there is no TAN utilization so higher carbon and NO_3-N use define phase one, and thus there is no phase two for this treatment.

Table 2.4: Description of the three phases of algal growth observed in each reactor treatment

Growth Phase	Reactor Treatment	Time Range (hr)	Peak Biomass (mg/L)	Nitrogen Source Used	Relative Carbon Availability	pH Trend
Phase One	Similar for all treatments	25.5-73.5	59.3[1]	TAN[2]	Peak for experiment duration	Slight decline, then increasing
Phase Two[3]	1.00 mM TAN, 1.00 mM NO_3-N	73.5-239	171.5	TAN	Low	Stable
	0.75 mM TAN, 1.25 mM NO_3-N	73.5-191.5	140.6			
	0.50 mM TAN, 1.50 mM NO_3-N	73.5-166.5	127.9			
Phase Three	1.00 mM TAN, 1.00 mM NO_3-N	239-433	322.7	NO_3-N	Low	Increasing
	0.75 mM TAN, 1.25 mM NO_3-N	191.5-433	351.1			
	0.50 mM TAN, 1.50 mM NO_3-N	166.5-433	466.1			
	0.25 mM TAN, 1.75 mM NO_3-N	73.5-384	447.8			
	0.00 mM TAN, 2.00 mM NO_3-N	73.5-384	440.5			

[1]Calculated by averaging the peak biomass for each reactor for this growth phase
[2]Excluding the 0.00 mM TAN, 2.00 mM NO_3-N reactor, in which NO_3-N was used during growth phase one
[3]Phase two is not applicable for the 0.25 mM TAN, 1.75 mM NO_3-N and 0.00 mM TAN, 2.00 mM NO_3-N reactor treatments

pH Effects

The sequential nature of nitrogen utilization can also be observed by the effect on pH, where autotrophic algal growth with NO_3-N consumes H^+ ions and raises the pH, while a TAN source results in the release of H^+ ions and lowers the pH (Markou et al., 2016). Visualized for each reactor in Figure 2.7, the pH remains somewhat constant during TAN concentration decline and substantially increases when NO_3-N concentration starts decreasing. The peak pH for each reactor increased with increasing initial NO_3-N concentration, with the NO_3-N only reactor (Figure 2.7e) reaching a maximum pH of 11.319. The 1 mM TAN, 1 mM NO_3-N reactor (Figure 2.7a) had a maximum pH of 10.990.

Early in phase one of growth, the pH sharply declines from the initially set pH of 10.3 at 25.5 hours. Initial CO_2 diffusion would be very fast as the mass transfer of CO_2 via a concentration gradient from atmospheric gas phase to liquid phase equalizes (Stumm & Morgan, 1981; Watson, 2009). At this point, total biomass is still very low, so CO_2 diffusion into the reactors is significantly greater than algal consumption. As CO_2 concentration increases, which is supported by the observed TIC peak at 25.5 hours, the pH declines with CO_2 hydration. Simultaneously, biomass is growing rapidly and consuming some TAN, which contributes to the initial pH drop also. After 25.5 hours, the pH sharply rises as acidic CO_2 is consumed by the increasing biomass combined with the conversion to HCO_3^- and CO_3^{2-} via CO_2 equilibria in aqueous systems at high pH (Stumm & Morgan, 1981).

Entering phase two of growth, the pH begins to stabilize where further pH decline was expected with TAN utilization. Biomass is still relatively low at approximately 20% of average maximum biomass concentration by the end of phase two, so TAN was being consumed and H^+ produced, but likely in small quantities. One hypothesis is that while TAN consumption tends to decrease pH, the effect was negated with further acidic CO_2 consumption that raised the pH, resulting in the observed plateau. Additionally with the low biomass, a large portion of the pH buffers in BG11 medium were still present to resist pH changes. In comparison to the NO_3-N only reactor at the same time range of phase two growth, pH steadily increases. Based on the stoichiometry of balanced chemical equations for algal growth with a CO_2 substrate (equations 2.1 and 2.2), 1.125 moles of H^+ are consumed per mole of NO_3^- consumed. Only 0.875 moles of H^+ are produced per mole of NH_4^+ consumed (Stumm & Morgan, 1981; 4), thus NO_3-N utilization contributes more to pH changes despite buffering effects from the growth medium.

With the phase three transition to NO_3-N utilization, pH increased as expected. The substantial pH increase during this period is most likely due to a much greater biomass production, with an average peak biomass for all reactors of 405.6 mg/L. A significant amount of phosphate and other buffers in the medium have been consumed by algae as nutrients, which might have also contributed to a reduced buffering capacity and more obvious pH effect.

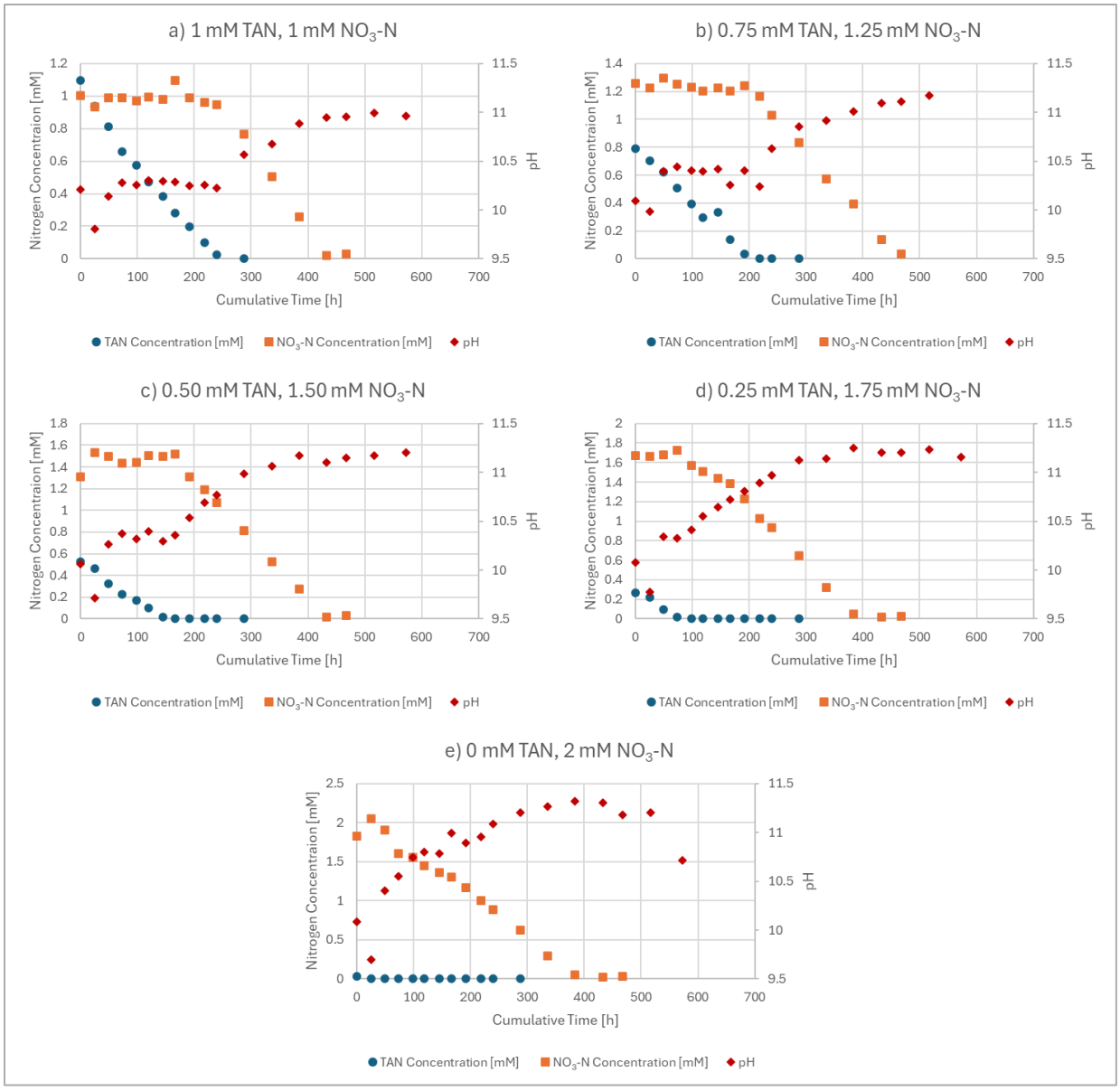

Figure 2.7: Nitrogen utilization and pH over time, with each reactor plotted in separate panels with letter designation a) through e)

Kinetic and Stoichiometric Growth Parameters

Specific Growth Rate

The natural log of biomass versus time for each reactor is plotted in Figure 2.8, delineated by the three prescribed growth phases. A linear trendline is applied for each

growth phase, with the slope representing the specific growth rate. In general, phase one specific growth rates are the fastest with visually steep slopes and phases two and three are significantly slower.

Surface level PAR readings were also plotted in Figure 2.8, which slightly decreased for all reactors as volume removal for sampling caused the surface liquid level in the reactors to decrease further away from the light source. There are two small increases in PAR, which are various magnitudes depending on the position of the reactors: at 73.5 hours, when lights were adjusted to lessen the differences in PAR between reactors, and at 191.5 hours, when a front bulb blew out and was replaced.

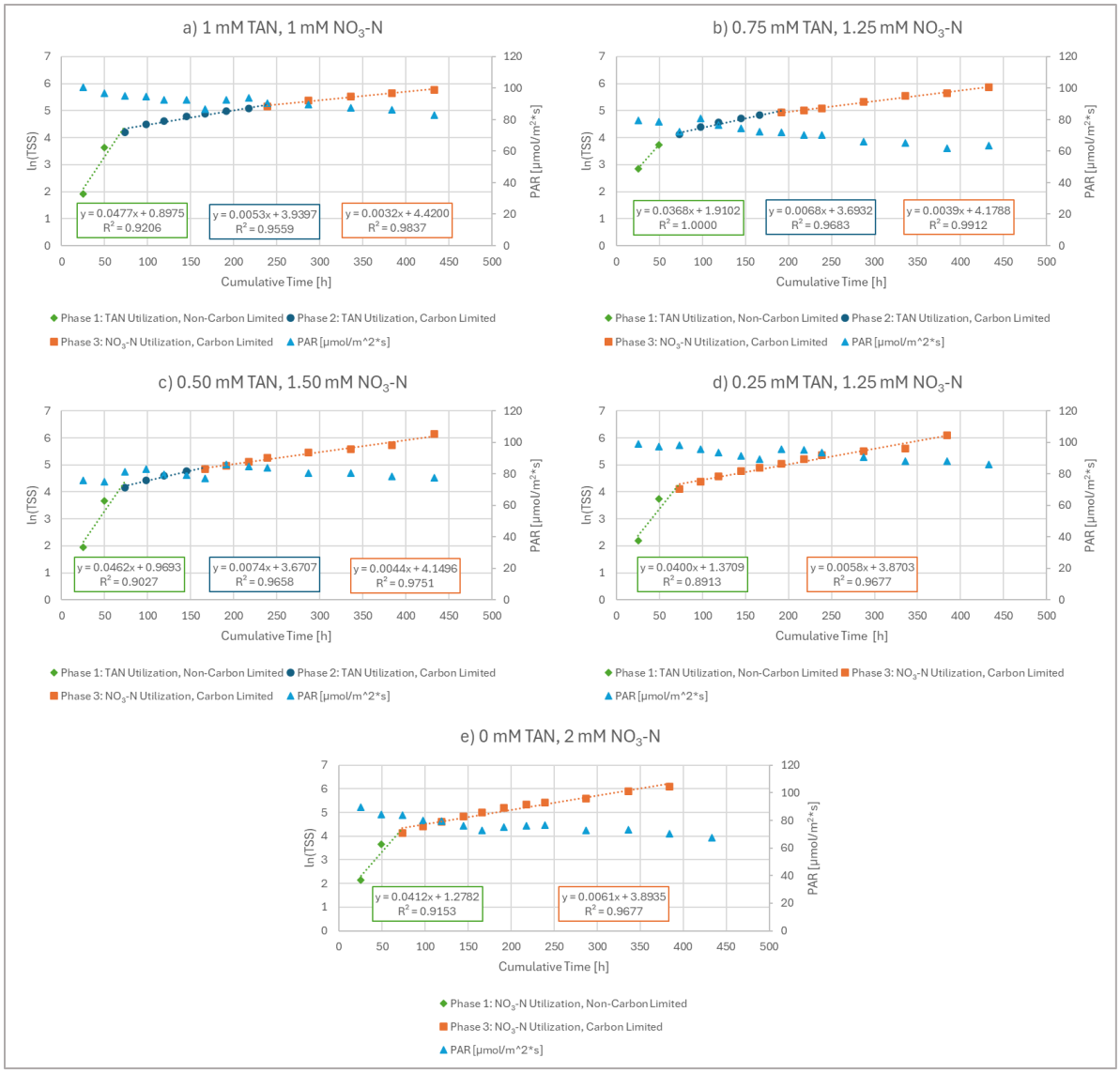

Figure 2.8: Natural log of biomass concentration and PAR over time, where the three phases of growth are indicated for each reactor. Each reactor is plotted in separate panels with letter designation a) through e).

The specific growth rates for each phase of growth from Figure 2.8 are compiled in Table 2.5 for each reactor. Subsequently, linear regressions (Figure 2.9) were used to investigate the impact of nitrogen source (TAN for phases one - two and NO_3-N for phase three) on growth rates. Statistical reports from IBM SPSS software analysis are included in Appendix C.

Table 2.5: Specific growth rates (μ) for the various reactor treatments, determined based on three growth phases

Reactor Treatment	Phase One μ (1/hr)	Phase Two μ (1/hr)	Phase Three μ (1/hr)
1.00 mM TAN, 1.00 mM NO_3-N	0.048	0.0053	0.0032
0.75 mM TAN, 1.25 mM NO_3-N	0.037	0.0068	0.0039
0.50 mM TAN, 1.50 mM NO_3-N	0.046	0.0074	0.0044
0.25 mM TAN, 1.75 mM NO_3-N	0.040	N/A[1]	0.0058
0.00 mM TAN, 2.00 mM NO_3-N	0.041	N/A[1]	0.0061

[1]Not applicable, no phase two growth for these reactor treatments

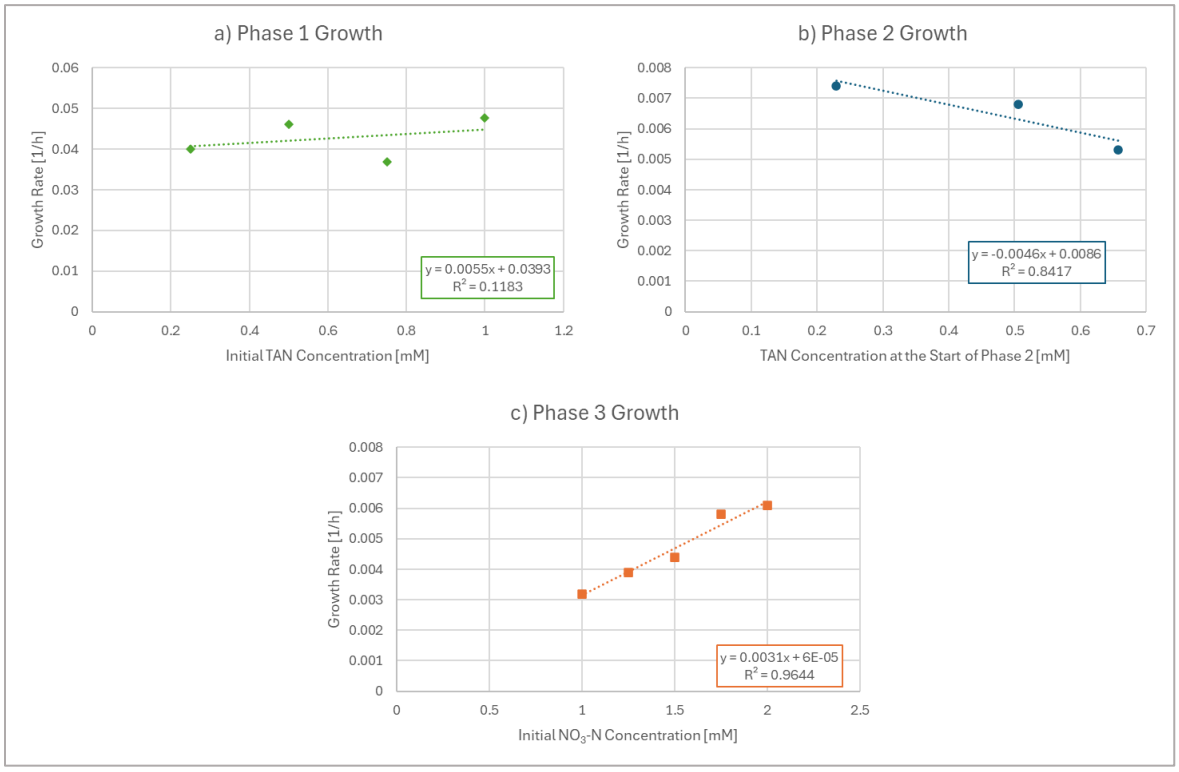

Figure 2.9: Linear regressions of specific growth rate and initial nitrogen substrate concentration, with each growth phase plotted in separate panels with letter designation a) through c)

During phase 1, initial TAN had no impact on specific growth rate. The linear regression between initial TAN and specific growth rate yielded a slope (0.0055 1/mM-hr) that was not significantly different than zero ($F(1,3) = 0.333$, $p = 0.622$). As such, the average specific growth rate during phase one when TAN was used as the sole nitrogen source was calculated as 0.043 hr^1.

During phase two, TAN at the start of phase two likely had an impact on specific growth rate. Initial TAN accounted for 84.2% of the variation in growth rate with an adjusted $R^2 = 0.683$. However, the linear regression between initial TAN and specific growth rate yielded a slope (-0.0046 1/mM-hr) that was not significantly different than zero ($F(1,2) = 5.316$, $p = 0.261$). It is possible that the slope was not statistically significant due to lack of statistical power, as only three of the five experimental reactors displayed a phase two growth rate (because all TAN was used in the earlier phase one or TAN was not provided in the reactor). Furthermore, decreasing specific growth rate with increase TAN is consistent with ammonia inhibition, which is known to occur for *Scenedesmus* (Abeliovich & Azov, 1976; Azov & Goldman, 1982).

During phase three, initial NO_3-N had a statistical impact on specific growth rate. Initial NO_3-N accounted for 96.4% of the variation in growth rate with an adjusted $R^2 = 0.953$. The linear regression between initial NO_3-N and specific growth rate yielded a slope (0.0031 1/mM-hr) that was significantly different than zero ($F(1, 4) = 81.22$, $p = 0.003$). As such, specific growth rate increased with increasing initial NO_3 during phase three when all TAN had already been exhausted and light and carbon were expected to have been limiting, due to high biomass production.

Nitrogen-Based Biomass Yield

Biomass yields were calculated for each reactor by either TAN or NO_3-N utilization, in which TSS was plotted versus nitrogen substrate concentration (Figure 2.10). A linear trendline is fitted to each period of nitrogen source use and the slope represents the biomass yield on a nitrogen basis. The yields are distinctly different for the two different nitrogen sources, with yield during TAN utilization being higher than NO_3-N utilization yields for all mixed reactors except the 0.75 mM TAN, 1.25 mM NO_3-N treatment. Biomass yield was also analyzed similarly to specific growth rate with three phases of growth, however, slopes during phases one and two were comparable since TAN consumption occurs during both (Appendix D).

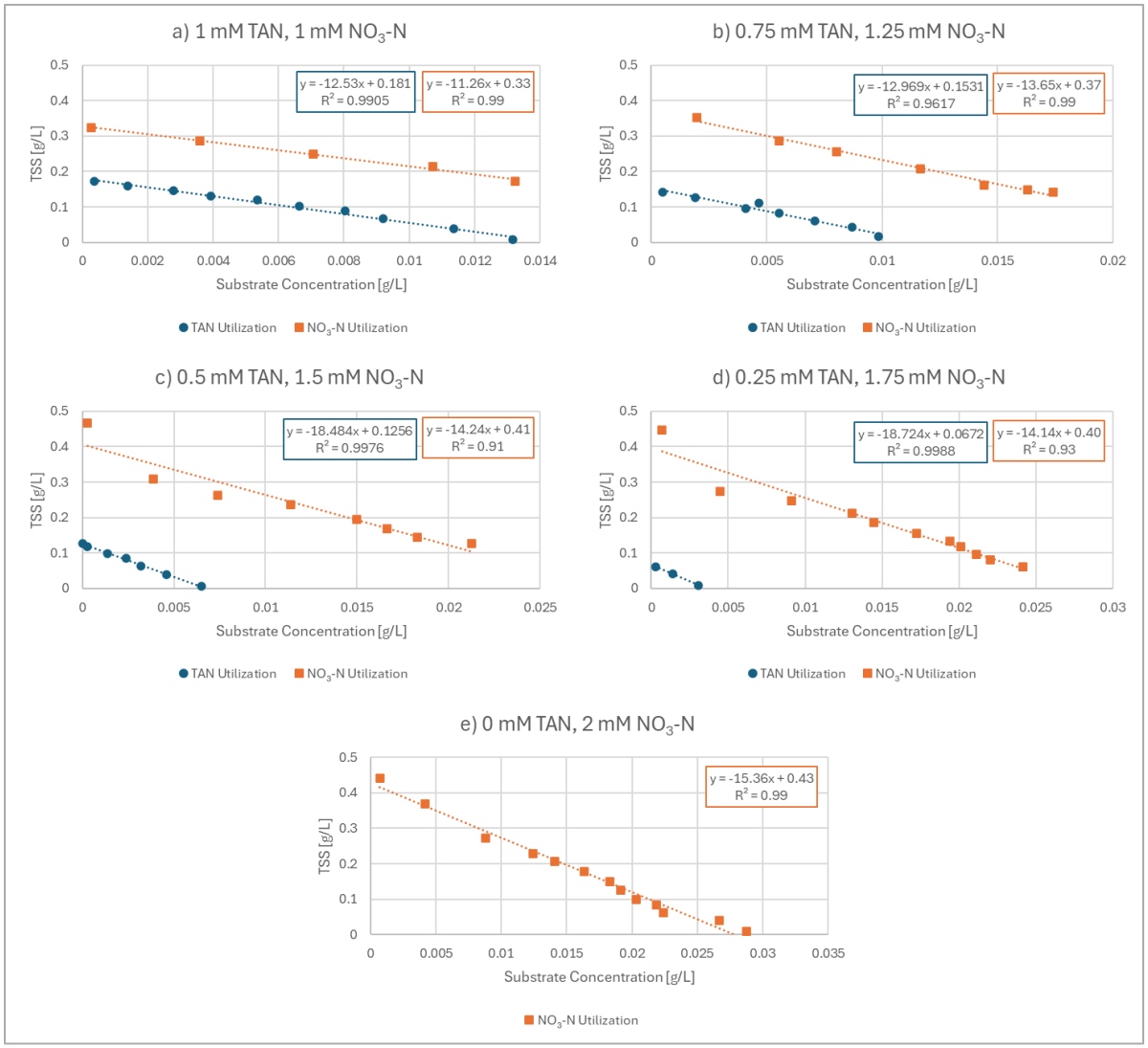

Figure 2.10: Biomass concentration over nitrogen substrate concentration, where TAN and NO_3-N utilization is indicated for each reactor. Each reactor is plotted in separate panels with letter designation a) through e).

Table 2.6 reports the biomass yields on a nitrogen basis for each reactor treatment. Linear regressions (Figure 2.11) were used to assess the effect of initial nitrogen source on biomass yields. Statistical reports from IBM SPSS software analysis are included in Appendix E.

Table 2.6: Biomass yields ($Y_{X/N}$) from experimental data, categorized by nitrogen source utilization

Reactor Treatment	TAN Utilization $Y_{X/N}$ (g/g)	NO_3-N Utilization $Y_{X/N}$ (g/g)
1.00 mM TAN, 1.00 mM NO_3-N	12.53	11.26
0.75 mM TAN, 1.25 mM NO_3-N	12.97	13.65
0.50 mM TAN, 1.50 mM NO_3-N	18.48	14.24
0.25 mM TAN, 1.75 mM NO_3-N	18.72	14.14
0.00 mM TAN, 2.00 mM NO_3-N	N/A[1]	15.36

[1]Not applicable since no TAN is provided for this reactor treatment

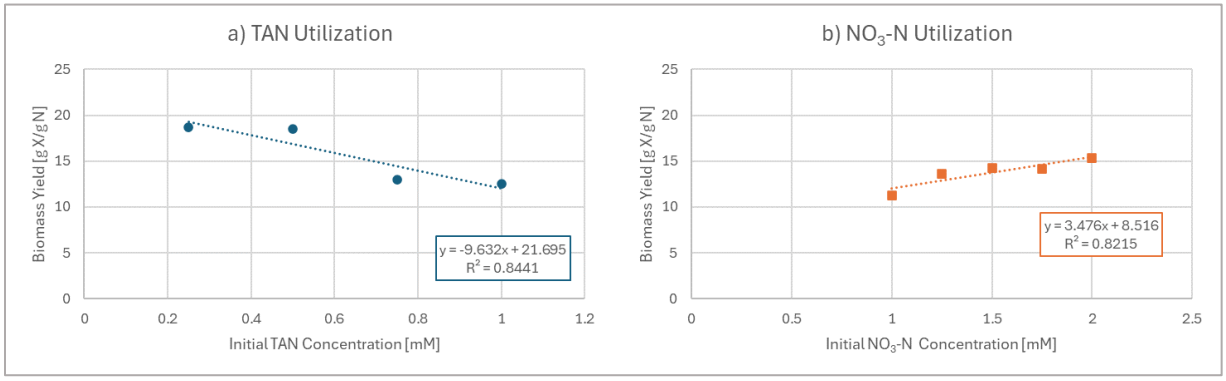

Figure 2.11: Linear regressions of biomass yield and initial substrate concentration, with TAN and NO_3-N utilization plotted in separate panels with letter designation a) and b), respectively

During TAN utilization, initial TAN likely had an impact on biomass yield. Initial TAN accounted for 84.8% of the variation in biomass yield with an adjusted $R^2 = 0.766$. However, the linear regression between initial TAN and biomass yield produced a slope (-9.632 1/mM) that was not significantly different than zero ($F(1,3) = 10.83$, $p = 0.081$). Biomass yield decreased with increasing TAN, potentially due to toxicity and growth inhibition (Abeliovich & Azov, 1976; Azov & Goldman, 1982).

During NO_3-N utilization, initial NO_3-N had a statistical impact on biomass yield. Initial NO_3-N accounted for 82.2% of the variation in biomass yield with an adjusted R^2 = 0.762. The linear regression between initial NO_3-N and biomass yield produced a slope (3.476 1/mM) that was significantly different than zero ($F(1,4) = 13.81$, $p = 0.034$). Biomass yield increased with increasing NO_3-N, which is not expected as biomass yield, being the ratio of cell mass to substrate mass, should be theoretically stable. This relationship could indicate that prior TAN utilization may have impacted results.

Biomass Elemental Composition

Biomass composition analysis was conducted on cells collected after 15 days (360 hours) of growth, well into phase three, NO_3-N consumption for all reactors. Elemental carbon constituted the greatest mass percentage of algal biomass in all reactors, ranging from 43.50-48.60% (Table 2.7). Carbon mass percentage showed a positive linear correlation ($R^2 = 0.8957$) with initial TAN concentration (Figure 2.12). It is possible that during phase one growth with non-limiting carbon or TAN use in which less metabolic energy is required, carbon reserve molecules accumulate. Then, the transition into a carbon-deficient environment coupled with NO_3-N utilization and a higher metabolic energy requirement induced a heterotrophic metabolism in some algae with the reserve molecules being metabolized (Weger et al., 1988; Collos & Harrison, 2014). Thus, carbon biomass percentages decrease with higher NO_3N treatments.

Biomass nitrogen and phosphorous mass percents were not significantly correlated with initial TAN concentration, and do not follow an evident trend; they

remain relatively stable across nitrogen treatments. A previous study by Watson (2009) evaluating the effects of varied TIC medium content also found nitrogen and phosphorus relatively constant.

Table 2.7: Elemental C:N:P ratios and molecular weights for each reactor treatment

Reactor Treatment	Carbon		Nitrogen		Phosphorous		Molecular Weight[1] (g/mol)
	%	mol	%	mol	%	mol	
1.00 mM TAN, 1.00 mM NO_3-N	48.50	51.38	8.80	8.00	2.43	1	1272.56
0.75 mM TAN, 1.25 mM NO_3-N	46.31	39.90	8.52	6.29	2.99	1	1034.88
0.50 mM TAN, 1.50 mM NO_3-N	46.88	37.93	8.93	6.19	3.19	1	971.89
0.25 mM TAN, 1.75 mM NO_3-N	44.62	37.49	8.50	6.12	3.07	1	1009.25
0.00 mM TAN, 2.00 mM NO_3-N	43.50	36.18	8.02	5.72	3.10	1	998.84

[1]Based on $(CH_2O)_x(NH_3)_y(H_3PO_4)$ algal molecular formula, in which x = mol C/mol P and y = mol N/mol P

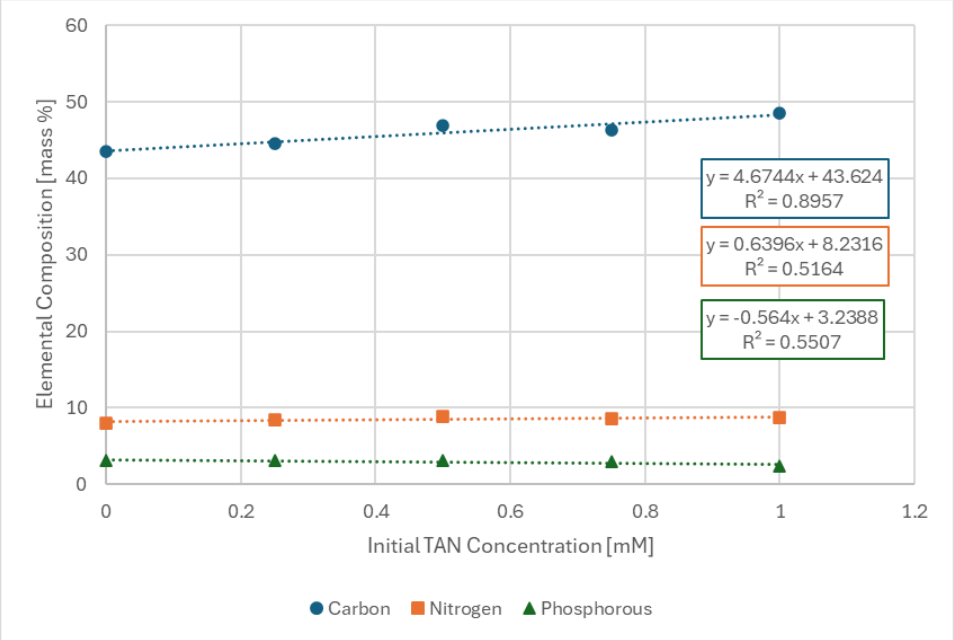

Figure 2.12: Carbon, nitrogen, and phosphorous elemental composition as a function of initial TAN concentrations

Of the other elements analyzed, calcium and magnesium mass percentages showed the highest correlation to initial TAN concentration (Figure 2.13). Both trace elements decrease with increasing initial TAN concentration. Studies show ammonia toxicity in higher plants results in cation depression, which could possibly be occurring through a similar mechanism in microalgae (Markou et al., 2016).

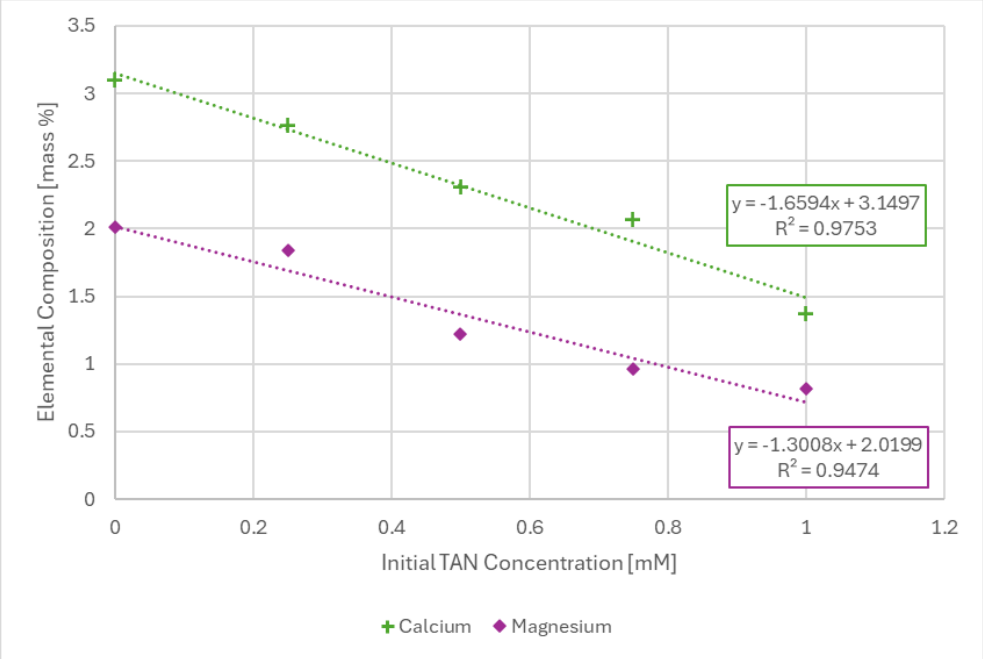

Figure 2.13: Elemental calcium and magnesium composition as a function of initial TAN concentrations

Conclusion

Removing excess atmospheric CO_2 through biological methods must be considered as a strategy to mitigate the effects of climate change and excessive CO_2 emissions. Algal uptake of inorganic carbon can approach maximum carbon removal efficiency by establishing the preferred nitrogen source of growth. In alignment with the

previously defined objectives, the main conclusions of this study are summarized as follows:

i. In reactors with mixed sources, nitrogen uptake is distinctly sequential, with TAN being utilized until total depletion first.

ii. Culture pH remains somewhat constant during TAN consumption and substantially increases when NO_3-N utilization begins, with peak pH for each reactor increasing with increasing initial NO_3-N concentration.

iii. For phase one growth, the average specific growth rate for growth when TAN was used as the sole nitrogen source under the highest inorganic carbon conditions was calculated as 0.043 hr^{-1}. Initial TAN likely had an impact on phase two specific growth rates, and initial NO_3-N had a statistically significant impact on phase three specific growth rates. Initial TAN and NO_3-N likely had an impact on biomass yields during their respective periods of utilization, but only the effect of initial NO_3-N on yield was statistically significant.

In an algal carbon capture system, pH control can be achieved by adding NO_3-N to raise pH for CO_2 diffusion enhancement or to lower pH with TAN addition in the case of an overly alkaline environment negatively impacting algal growth. Future research is needed to determine kinetic parameters, such as maximum specific growth rates and half-saturation constants for TAN and NO_3-N only growth, and to prevent the additional carbon limitation effects. Carbon limitation could be avoided by allowing reactors to

reach CO_2 saturation prior to inoculation, or by adding an initial external inorganic carbon source.

References

Abeliovich, A., & Azov, Y. (1976). Toxicity of ammonia to algae in sewage oxidation ponds. *Applied and Environmental Microbiology*, *31*(6), 801–806. https://doi.org/10.1128/aem.31.6.801-806.1976

Adams, C., & Bugbee, B. (2014). Nitrogen retention and partitioning at the initiation of lipid accumulation in nitrogen-deficient algae. *Journal of Phycology*, *50*(2), 356–365. https://doi.org/10.1111/jpy.12167

APHA (1995) Standard Methods for the Examination of Water and Wastewater. 19th Edition, American Public Health Association Inc., New York.

Azov, Y., & Goldman, J. C. (1982). Free ammonia inhibition of algal photosynthesis in intensive cultures. *Applied and Environmental Microbiology*, *43*(4), 735–739. https://doi.org/10.1128/aem.43.4.735-739.1982

Collos, Y., & Harrison, P. J. (2014). Acclimation and toxicity of high ammonium concentrations to unicellular algae. *Marine Pollution Bulletin*, *80*(1–2), 8–23. https://doi.org/10.1016/j.marpolbul.2014.01.006

Crofts, A. R. (1966). Uptake of ammonium ion by chloroplasts, and the mechanism of amine uncoupling. *Biochemical and Biophysical Research Communications*, *24*(1), 127–134. https://doi.org/10.1016/0006-291x(66)90420-7

Drapcho, C. M., Nhuan, N. P., & Walker, T. H. (2020). *Biofuels Engineering Process Technology*. McGraw-Hill.

Farrelly, D. J., Everard, C. D., Fagan, C. C., & McDonnell, K. P. (2013). Carbon sequestration and the role of Biological Carbon Mitigation: A Review. *Renewable and Sustainable Energy Reviews*, *21*, 712–727. https://doi.org/10.1016/j.rser.2012.12.038

IBM Corp. Released 2020. IBM SPSS Statistics for Windows, Version 27.0. Armonk, NY: IBM Corp

Lachmann, S. C., Mettler-Altmann, T., Wacker, A., & Spijkerman, E. (2019). Nitrate or ammonium: Influences of nitrogen source on the physiology of a green alga. *Ecology and Evolution*, *9*(3), 1070–1082. https://doi.org/10.1002/ece3.4790

Laerd Statistics (2015). *Statistical tutorials and software guides*. Retrieved from https://statistics.laerd.com/

Lee, J.-Y., J. Marotzke, G. Bala, L. Cao, S. Corti, J.P. Dunne, F. Engelbrecht, E. Fischer, J.C. Fyfe, C. Jones, A. Maycock, J. Mutemi, O. Ndiaye, S. Panickal, and T. Zhou, 2021: Future Global Climate: Scenario-Based Projections and Near-Term Information. In Climate Change 2021: The Physical Science Basis. Contribution of Working Group I to the Sixth Assessment Report of the Intergovernmental Panel on Climate Change (Masson-Delmotte, V., P. Zhai, A. Pirani, S.L. Connors, C. Péan, S. Berger, N. Caud, Y. Chen, L. Goldfarb, M.I. Gomis, M. Huang, K. Leitzell, E. Lonnoy, J.B.R. Matthews, T.K. Maycock, T. Waterfield, O. Yelekçi, R. Yu, and B. Zhou (eds.)). Cambridge University Press, Cambridge, United Kingdom and New York, NY, USA, pp. 553–672, doi: 10.1017/9781009157896.006.

Li, Y., Horsman, M., Wang, B., Wu, N., & Lan, C. Q. (2008). Effects of nitrogen sources on cell growth and lipid accumulation of green alga Neochloris Oleoabundans. *Applied Microbiology and Biotechnology*, *81*(4), 629–636. https://doi.org/10.1007/s00253-008-1681-1

Markou, G., Depraetere, O., & Muylaert, K. (2016). Effect of ammonia on the photosynthetic activity of Arthrospira and chlorella: A study on chlorophyll fluorescence and Electron Transport. *Algal Research*, *16*, 449–457. https://doi.org/10.1016/j.algal.2016.03.039

Sanz-Luque, E., Chamizo-Ampudia, A., Llamas, A., Galvan, A., & Fernandez, E. (2015). Understanding nitrate assimilation and its regulation in microalgae. *Frontiers in Plant Science*, *6*. https://doi.org/10.3389/fpls.2015.00899

Sayre, R. (2010). Microalgae: The potential for Carbon Capture. *BioScience*, *60*(9), 722–727. https://doi.org/10.1525/bio.2010.60.9.9

Stumm, W., & Morgan, J. J. (1981). *Aquatic chemistry: An introd. emphasizing chemical equilibria in natural waters*. Wiley.

Thermo Scientific. (2010). User Guide High Performance Ammonia Ion Selective Electrode.

Todd, L. J., Watson, M. K., & Drapcho, C. M. (2024). Quantification of inorganic carbon at high pH in BG11 algal growth media. Manuscript in preparation.

Watson, M. K. (2009). (thesis). *Growth and modeling of freshwater algae as a function of media inorganic carbon content*.

Watson, M. K., Flanagan, E., & Drapcho, C. M. (2024). Inorganic carbon-limited freshwater algal growth at high pH: revised with focus on alkalinity. Manuscript in preparation.

Weger, H. G., Birch, D. G., Elrifi, I. R., & Turpin, D. H. (1988). Ammonium assimilation requires mitochondrial respiration in the light. *Plant Physiology*, *86*(3), 688–692. https://doi.org/10.1104/pp.86.3.688

Wet ashing procedure for using HNO3+30%H202 for determining p, K, ca, Mg, Zn, Mn, Cu, Fe, S. Wet Ashing Procedure for using HNO3+30%H202 for Determining P, K, Ca, Mg, Zn, Mn, Cu, Fe, S | Public | Clemson University, South Carolina. (n.d.). https://www.clemson.edu/public/regulatory/ag-srvc-lab/feed-forage/procedure6.html

APPENDICES

Appendix A

TAN Volatilization and Temperature Analysis

To quantify TAN volatilization, two glass reactors of four-liter liquid volume were prepared with modified BG11 growth medium (Table 2.1) initially adjusted to the highest observed experimental pH of 11.5. The two initial TAN treatments were 1 mM and 0.25 mM. The reactors were set up identically to the experimental design described in Chapter Two, except with no algal inoculation. TAN was measured every five hours for the first day and then daily for a total 284 hours.

The measured TAN concentration is plotted over time for the two reactors in Figure A.1. The 1 mM TAN reactor had a 4.37 mg/L decrease in TAN over the 284 hours, while the 0.25 mM TAN reactor had a 1.35 mg/L decrease. During algal growth experimentation, the pH remained stable and below 10.5 for all reactors during TAN utilization, so it is likely that any volatilization was less than the observed loss at pH 11.5.

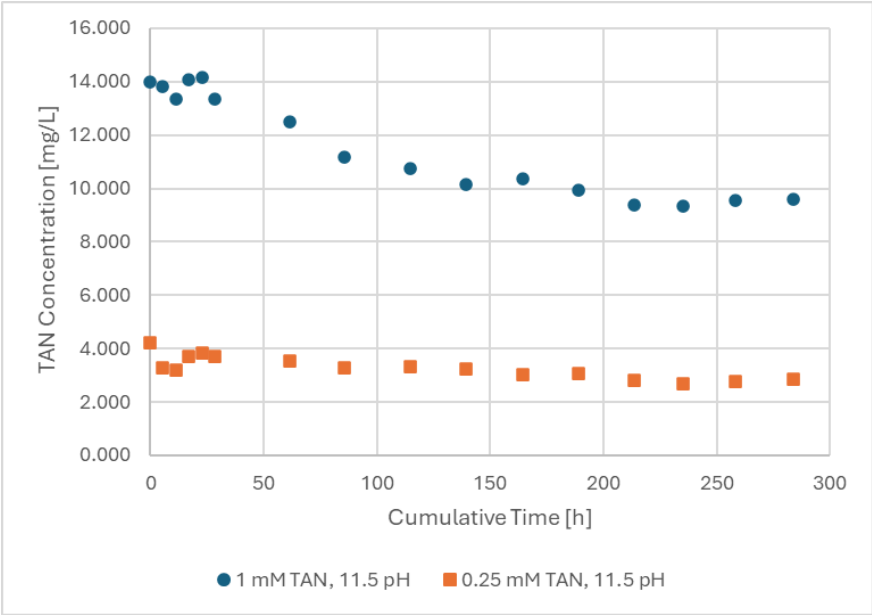

Figure A.1: TAN Concentration versus time for two initial TAN treatments at 11.5 pH

To determine if temperature correction during TAN measurement was necessary, five TAN standards in BG11 growth medium were measured with and without an Automatic Temperature Compensation (ATC) probe. The results in Table A.1 indicate that percent error without temperature correction is comparable to percent error with temperature correction, and thus was not necessary for the algal growth study in Chapter Two.

Table A.1: Comparison of measured TAN concentration with and without temperature corrections

	Mean Measured TAN ± Standard Deviation of Technical Replicates (mg/L)		**Percent Error**	
Added TAN (mg/L)	Without Temperature Correction	With Temperature Correction	Without Temperature Correction	With Temperature Correction
2.5	2.9 ± 0.0	2.8 ± 0.0	15.7%	13.8%
12.3	12.5 ± 0.1	12.5 ± 0.1	1.3%	1.3%
24.7	24.3 ± 0.1	24.3 ± 0.0	1.4%	1.6%
61.1	60.2 ± 0.3	60.3 ± 0.2	2.3%	2.1%
246.6	244.3 ± 1.4	244.5 ± 2.1	0.9%	0.7%

Appendix B

Ion Chromatograph Flow Rate and NO_3^- Peak Area Analysis

To determine the optimal flow rate for best anion peak separation, eluent flow rates of 0.50, 0.75, and 1 mL/min were tested with multiple NO_3^- standards. The concentration of all samples was kept below 20 mg/L NO_3^- to not overload anion column, which was accomplished via serial dilution. An example of the difference between the flow rates for one standard concentration of 8.5 mg/L NO_3^- is shown in Figure B.1. The chromatographs have been offset by their response values for easier comparison. To the right of each NO_3^- peak, there is another smaller peak which represents other anions in the medium. With lower flow rates, there is better separation between these peaks, so an eluent flow rate of 0.50 mL/min was chosen for analyzation of samples.

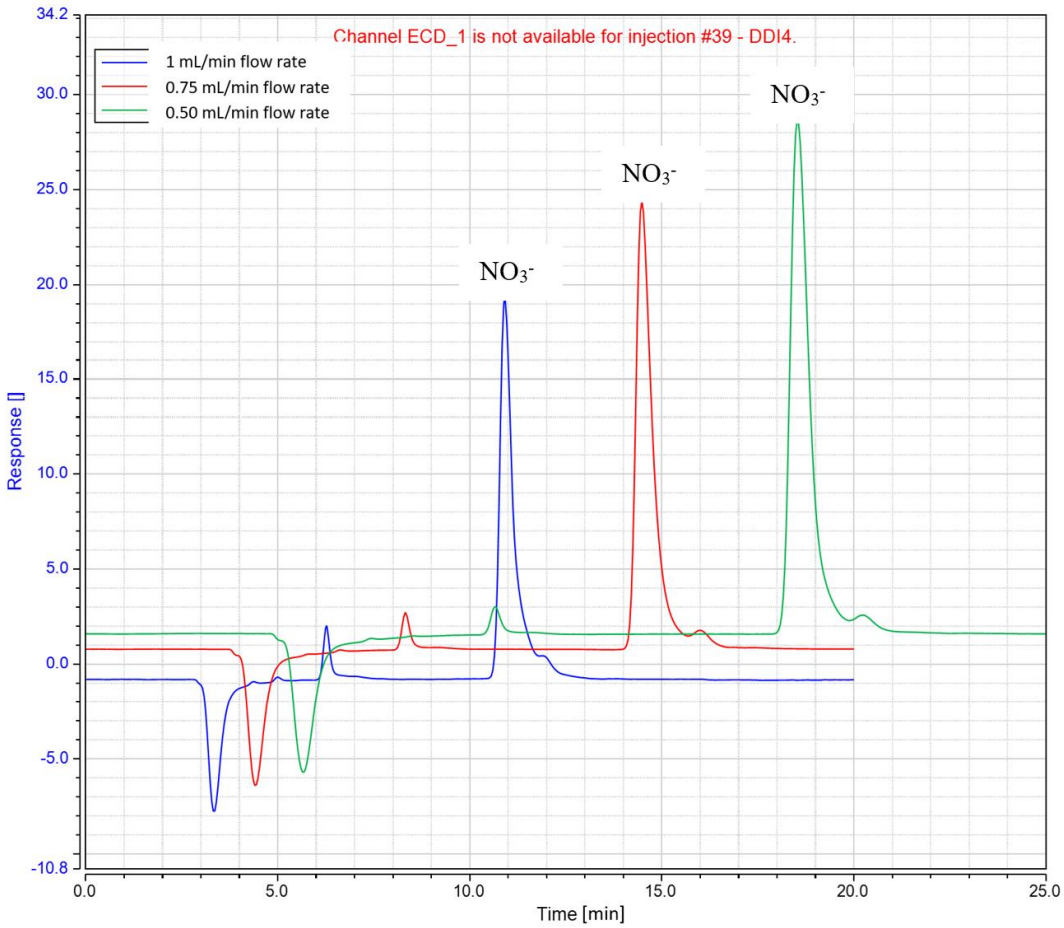

Figure B.1: Chromatographs for an 8.5 mg/L NO_3^- standard in BG11 growth medium with three different eluent flow rates. The NO_3^- peak is labeled for each chromatograph.

Experimental samples were diluted to approximately 8 mg/L NO_3^- to allow for a middle point between calibration standards in case of fluctuations and potential reduction of dilutions later during algal growth as NO_3^- is consumed. For the maximum NO_3^- concentration of 124.0 mg/L, this is a four-fold dilution. In Figure B.2, chromatographs of various NO_3^- standards based on three-, four-, five-, and six-fold dilutions of the maximum experimental concentration were used to inform the number of dilutions needed during experimentation.

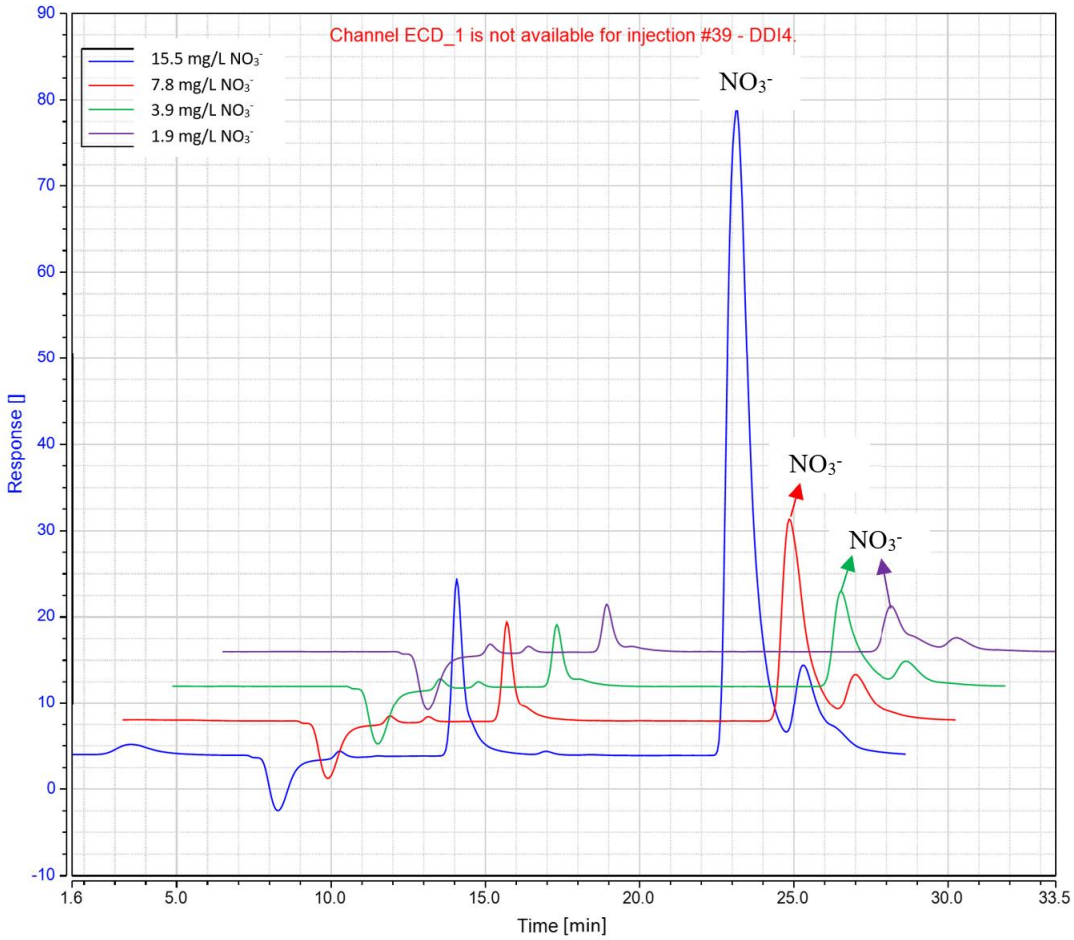

Figure B.2: Chromatographs for 1.9, 3.9, 7.8, and 15.5 mg/L NO_3^- standards in BG11 medium. The NO_3^- peak is labeled for each chromatograph.

Appendix C

IBM SPSS Reports for Specific Growth Rates and Biomass Yields

Phase One Specific Growth Rates

Table C.1: Model summary output for linear regression of phase one specific growth rates versus initial TAN

Model	R	R Square	Adjusted R Square	Std. Error of the Estimate
1	.378[a]	.143	-.286	.0058095

Table C.2: ANOVA output for linear regression of phase one specific growth rates versus initial TAN

Model		Sum of Squares	df	Mean Square	F	Sig.
1	Regression	.000	1	.000	.333	.622[b]
	Residual	.000	2	.000		
	Total	.000	3			

Table C.3: Coefficients output for linear regression of phase one specific growth rates versus initial TAN

Model		Unstandardized Coefficients		Standardized Coefficients	t	Sig.
		B	Std. Error	Beta		
1	(Constant)	.039	.007		5.481	.032
	InitialTAN	.006	.010	.378	.577	.622

Phase Two Specific Growth Rates

Table C.4: Model summary output for linear regression of phase two specific growth rates versus initial TAN

Model	R	R Square	Adjusted R Square	Std. Error of the Estimate
1	.917[a]	.842	.683	.0006087

Table C.5: ANOVA output for linear regression of phase two specific growth rates versus initial TAN

Model		Sum of Squares	df	Mean Square	F	Sig.
1	Regression	.000	1	.000	5.316	.261[b]
	Residual	.000	1	.000		
	Total	.000	2			

Table C.6: Coefficients output for linear regression of phase two specific growth rates versus initial TAN

Model		Unstandardized Coefficients		Standardized Coefficients	t	Sig.
		B	Std. Error	Beta		
1	(Constant)	.009	.001		8.757	.072
	TAN2	-.005	.002	-.917	-2.306	.261

Phase Three Specific Growth Rates

Table C.7: Model summary output for linear regression of phase three specific growth rates versus initial NO_3-N

Model	R	R Square	Adjusted R Square	Std. Error of the Estimate
1	.982[a]	.964	.953	.0002702

Table C.8: ANOVA output for linear regression of phase three specific growth rates versus initial NO_3-N

Model		Sum of Squares	df	Mean Square	F	Sig.
1	Regression	.000	1	.000	81.219	.003[b]
	Residual	.000	3	.000		
	Total	.000	4			

Table C.9: Coefficients output for linear regression of phase three specific growth rates versus initial NO_3-N

Model		Unstandardized Coefficients		Standardized Coefficients	t	Sig.
		B	Std. Error	Beta		
1	(Constant)	6.000E-5	.001		.114	.916
	InitialNO3	.003	.000	.982	9.012	.003

TAN Utilization Biomass Yields

Table C.10: Model summary output for linear regression of TAN utilization biomass yields versus initial TAN

Model	R	R Square	Adjusted R Square	Std. Error of the Estimate
1	.906[a]	.822	.762	.7395472

Table C.11: ANOVA output for linear regression of TAN utilization biomass yields versus initial TAN

Model		Sum of Squares	df	Mean Square	F	Sig.
1	Regression	7.552	1	7.552	13.807	.034[b]
	Residual	1.641	3	.547		
	Total	9.192	4			

Table C.12: Coefficients output for linear regression of TAN utilization biomass yields versus initial TAN

Model		Unstandardized Coefficients		Standardized Coefficients	t	Sig.
		B	Std. Error	Beta		
1	(Constant)	8.516	1.442		5.907	.010
	InitialNO3	3.476	.935	.906	3.716	.034

NO_3-N Utilization Biomass Yields

Table C.13: Model summary output for linear regression of NO_3-N utilization biomass yields versus initial NO_3-N

Model	R	R Square	Adjusted R Square	Std. Error of the Estimate
1	.919[a]	.844	.766	1.6364260

Table C.14: ANOVA output for linear regression of NO_3-N utilization biomass yields versus initial NO_3-N

Model		Sum of Squares	df	Mean Square	F	Sig.
1	Regression	28.992	1	28.992	10.827	.081[b]
	Residual	5.356	2	2.678		
	Total	34.348	3			

Table C.15: Coefficient output for linear regression of NO_3-N utilization biomass yields versus initial NO_3-N

Model		Unstandardized Coefficients		Standardized Coefficients		
		B	Std. Error	Beta	t	Sig.
1	(Constant)	21.695	2.004		10.825	.008
	InitialTAN	-9.632	2.927	-.919	-3.290	.081

Appendix D

Biomass Yield Analysis for Three Growth Phases

In Figure D.1, biomass yield was analyzed based on the three defined growth phases. For the reactors in panels a through c, phases one and two are defined by TAN utilization. The biomass yields for these two phases are compiled in Table D.1 for the following reactors: 1 mM TAN:1 mM NO_3-N, 0.75 mM TAN:1.25 mM NO_3-M, and 0.5 mM TAN:1.5 mM NO_3-N. Statistical reports from IBM SPSS software analysis are included in the following tables.

A paired-samples t-test was used to determine whether there was a statistically significant mean difference between the biomass yields in phase one compared to phase two. The null hypothesis for the paired-samples t-test is the population mean difference between phase one and phase two biomass yields is equal to zero. The alternative hypothesis is the population mean difference between phase one and phase two biomass yields is not equal to zero. No outliers were detected from the boxplot (Figure D.2). The assumption of normality was not violated, as assessed by Shapiro-Wilk's test ($p = 0.944$) (Table D.2). There was not a statistically significant difference between means ($p = 0.339$) and therefore, we must reject the alternative hypothesis and fail to reject the null hypothesis (Table D.3). Thus, biomass yields in Chapter Two were categorized by nitrogen utilization instead of growth phases.

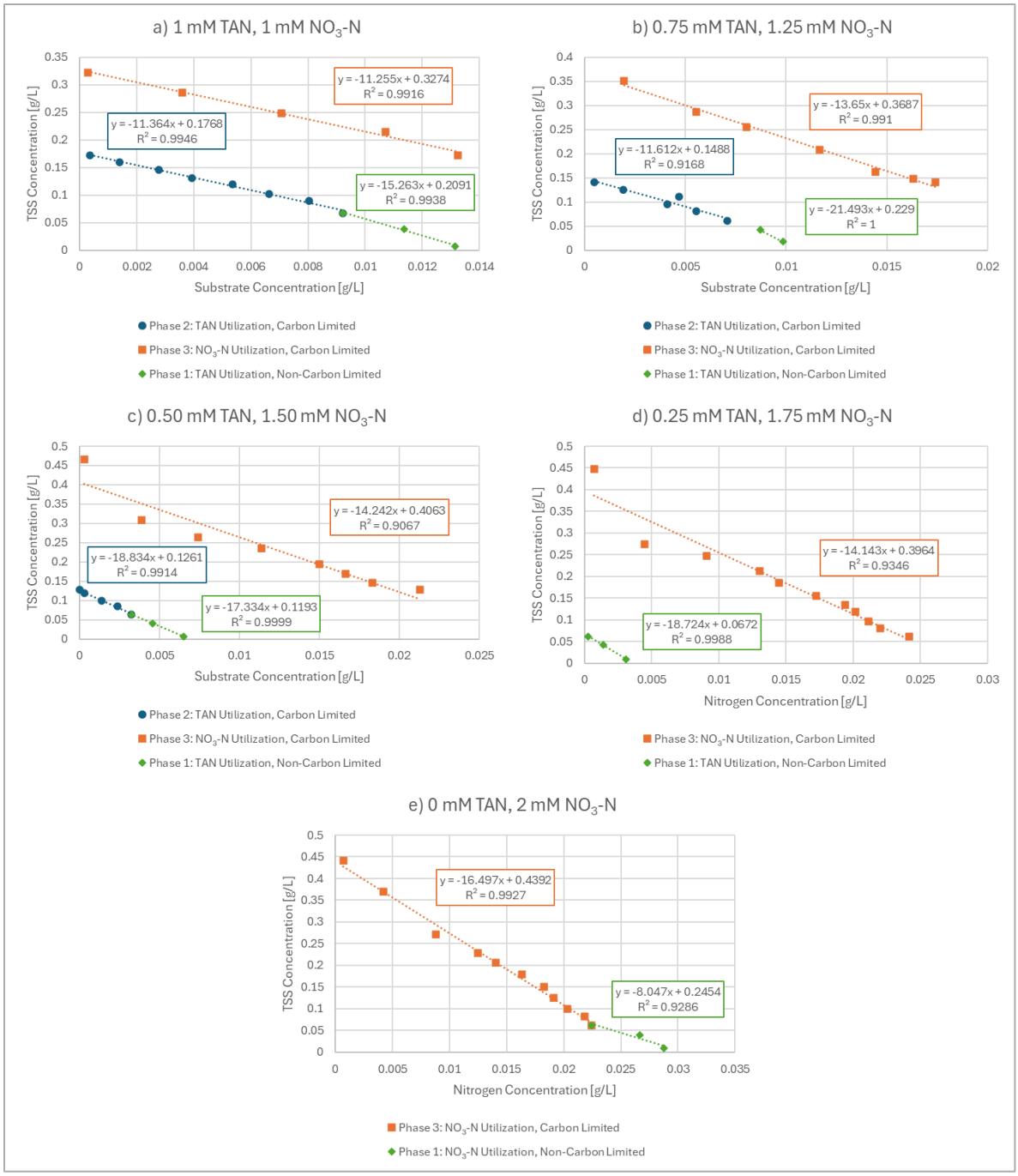

Figure D.1: Biomass concentration over nitrogen concentration, where the three phases of growth are indicated for each reactor. Each reactor is plotted in separate panels with letter designation a) through e).

Table D.1: Biomass yields ($Y_{X/N}$) from experimental data, with TAN utilization categorized by growth phases one and two

Reactor Treatment[1]	Phase One $Y_{X/N}$ (g/g)	Phase Two $Y_{X/N}$ (g/g)
1.00 mM TAN, 1.00 mM NO_3-N	15.26	11.36
0.75 mM TAN, 1.25 mM NO_3-N	21.49	11.61
0.50 mM TAN, 1.50 mM NO_3-N	17.33	18.83

[1]There is no growth phase two for the 0.25 mM TAN, 1.75 mM NO_3-N and 0 mM TAN, 2 mM NO_3-N reactors

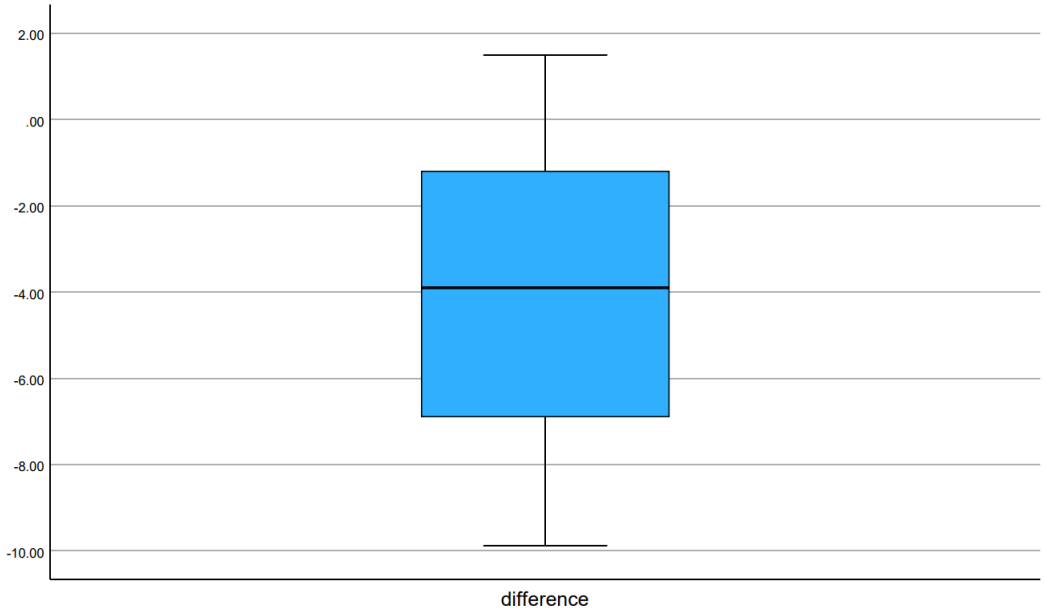

Figure D.2: Boxplot of the difference between phase two and phase one biomass yields, used to determine outliers

Table D.2: Tests of Normality output for the difference between phase two and phase one biomass yields, used to determine normality

	Kolmogorov-Smirnov[a]			Shapiro-Wilk		
	Statistic	df	Sig.	Statistic	df	Sig.
difference	.180	3	.	.999	3	.944

a. Lilliefors Significance Correction

Table D.3: Paired Samples Test output for a paired-samples t-test with biomass yields from growth phases one and two

		Paired Differences					t	df	Significance	
					95% Confidence Interval of the Difference					
		Mean	Std. Deviation	Std. Error Mean	Lower	Upper			One-Sided p	Two-Sided p
Pair 1	Y1 - Y2	4.0933333	5.6929882	3.2868483	-10.0488333	18.2354999	1.245	2	.170	.339

Appendix E

OD versus TSS Standard Curves

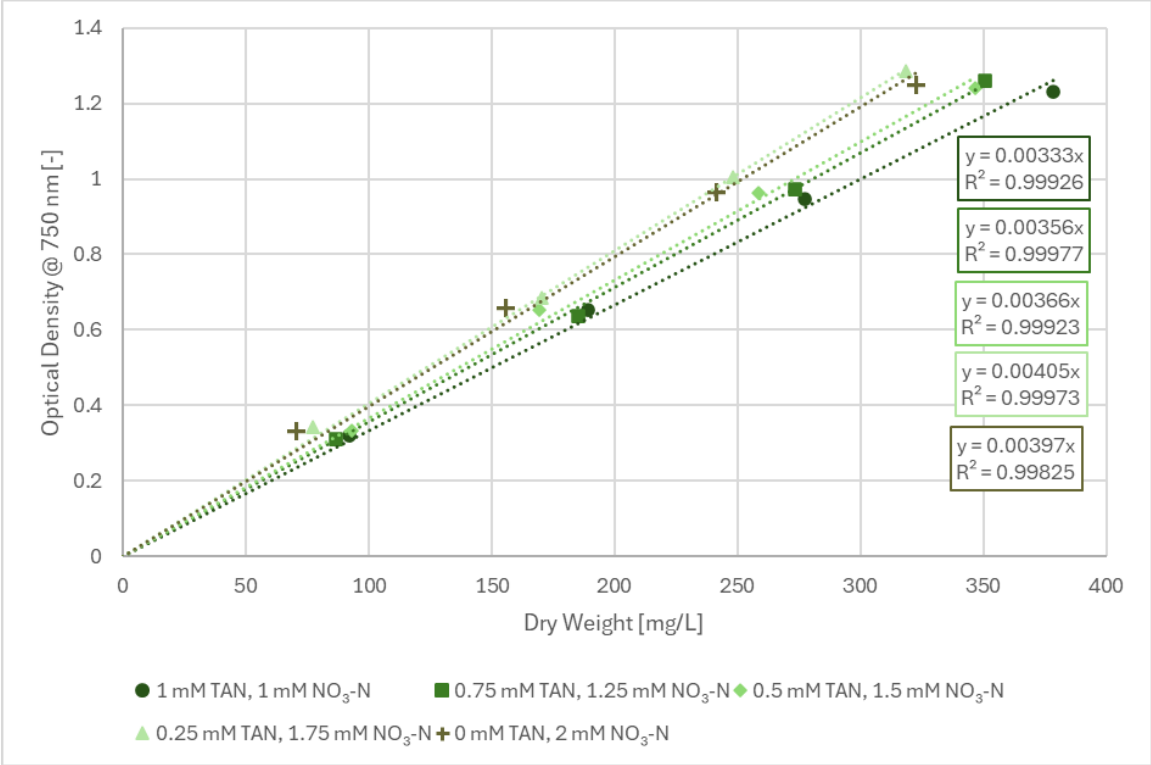

Figure E.1: OD versus TSS standard curve for the five experimental nitrogen treatments